UNIVERSITY OF CALIFORNIA,
IRVINE

Muon Telescope and TPC Data Analysis for mini-CAPTAIN

THESIS

submitted in partial satisfaction of the requirements
for the degree of

MASTER OF SCIENCE

in Physics

by

Craig William Pitcher

Thesis Committee:
Professor Henry Sobel, Chair
Professor Arvind Rajaraman
Professor Tim Tait

2015

TABLE OF CONTENTS

Page

LIST OF FIGURES

Page

LIST OF TABLES

Page

ACKNOWLEDGMENTS

special thanks

to

my

advisor

Michael Smy

ABSTRACT OF THE THESIS

Muon Telescope and TPC Data Analysis for mini-CAPTAIN

By

Craig William Pitcher

Master of Science in Physics

University of California, Irvine, 2015

Professor Henry Sobel, Chair

Mini-CAPTAIN is a 400 kg liquid argon time projection chamber (TPC) and serves as a prototype for the 5 ton CAPTAIN detector. Cosmic muons are the primary data source for its commissioning phase. These particles are tracked by the muon telescope, consisting of multi-wire chambers for data collection and scintillator paddles for triggering. Telescope event reconstruction, track extrapolation into the TPC, and correlation of events between these two detector systems will be discussed. I will demonstrate that telescope events can be used to calculate which TPC wires are good candidates for seeing a muon signal. While a full muon track has not yet been seen in TPC data due to high electronic noise and insufficient liquid argon purity, the analysis programs detailed in this paper will expedite track finding once new data has been collected. This work can also be used to align the TPC before it takes data in a beam.

CHAPTER 1: INTRODUCTION

1.1 Previous and Upcoming Neutrino Experiments

After Frederick Reines discovered the neutrino in 1956, dozens of experiments all over the globe have studied this elusive particle. One important tool used in many neutrino experiments is the liquid argon time projection chamber (LAr TPC). For a discussion on the physics behind a LAr TPC, refer to section 1.4. These detectors can be used to track particles with millimeter precision, deduce particle energy loss over a distance, and determine a particle's identity. For these reasons and more, liquid argon TPCs have played an important role in neutrino physics experiments. The full potential of LAr detectors has not been realized, as current and upcoming experiments will employ the largest LAr detectors to date and explore some of the most important questions in neutrino physics.

The first major neutrino experiment to use LAr TPC technology was ICARUS (Imaging Cosmic And Rare Underground Signals), initiated in 1977 [1]. ICARUS initially focused on obtaining large electron drift distances in liquid argon. This has been an important, on-going experiment with consistent publications from 1985 to 2013. In light of ICARUS's success, several other experiments using LAr TPCs have come to fruition, of which I will focus on the recent collaborations formed at The Fermi National Accelerator Laboratory (Fermilab) and Los Alamos National Laboratory (LANL).

Fermilab is currently hosting the neutrino-focused collaborations MicoBooNE and MINERvA. Both are working with a collaboration based at LANL called CAPTAIN (Cryogenic Apparatus for Precision Tests of Argon Interactions with Neutrinos). A nearly identical electronics system to CAPTAIN's is currently being tested by MicroBooNE at Fermilab.

MicroBooNE also compliments the CAPTAIN experiment since it will study neutrinos of a lower energy range than CAPTAIN, and therefore the collective effort captures a broader energy spectrum of neutrinos.

While CAPTAIN is independently important, it is supportive of a next-generation neutrino experiment called the Long Baseline Neutrino Facility (LBNF) at Fermilab. A high intensity neutrino beam is generated at Fermilab. This beam is intercepted by both a near detector and a massive 40 kton far detector that is 1,300 km downstream at the Sanford Underground Research Facility (SURF) in Lead, SD [2]. Having two detectors separated by a large distance like this gives rise to the term "long baseline." The neutrino beam is generated by stopped pions that decay into a muons and muon neutrinos. Depending on the sign of the pions, either a neutrino or an anti-neutrino beam is generated. Measurements on both beam types allows for searches of charge-parity (CP) violation, an important topic in particle physics that may give a fundamental explanation for the matter-antimatter asymmetry in the universe.

The long term plans for CAPTAIN and MINERvA coincide, and signifying the joint effort is the CAPTAIN-MINERvA group. The detectors for these two experiments will eventually be moved next to each other in a beam line at Fermilab [3], where CAPTAIN will track particles and MINERvA will perform calorimetry. To do so, MINERvA is placed just past the CAPTAIN detector and filled with a dense material, thereby absorbing particles and measuring their energy.

The Deep Underground Neutrino Experiment (DUNE) collaboration was formed in early 2015 to take on the experimental program of LBNF, which includes building a 40 kton LAr detector and analyzing the vast amount of data. It will be several years before

construction begins for the new facilities at SURF and Fermilab. Ten years or more of data will be required to realize the main physics goals of the experiment since neutrino interactions are so rare, even using the world's highest intensity neutrino beam and the world's largest LAr detector.

Aspects of LBNF and DUNE depend on the success of CAPTAIN and mini- CAPTAIN; therefore, CAPTAIN is a vital program for research and development. Incremental progress through smaller-scale experiments ensures that important interaction backgrounds are understood and that the electronic systems successfully take data and monitor vital signs of the experiment. In running the CAPTAIN experiment, methods for calibration and analysis can also be developed in advance to expedite the physics results. Just as importantly, adjustments can be made to maximize the impact and success of LBNF and DUNE.

1.2 CAPTAIN Background and Physics Goals

The CAPTAIN detector is a 7,700 liter liquid argon cryostat containing a TPC, laser calibration system, and photon detection system [4]. This detector is currently housed at Los Alamos National Laboratory (LANL) but is designed to be portable. A drawing of the detector is shown in figure 1.1 on the next page.

During the initial runs, cosmic muon and laser data will be used to calibrate and commission the detector. This is also the case for mini-CAPTAIN. In the next phase, CAPTAIN will be moved to a high intensity neutron beam that is part of the Los Alamos Neutron Science Center. The last phase is to move the detector into a neutrino beam, most notably neutrino sources at Fermilab or Oak Ridge National Laboratory [4].

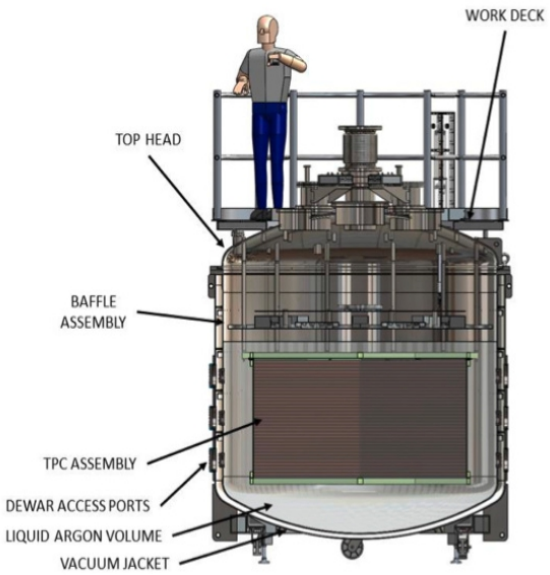

Figure 1.1 – The CAPTAIN Detector

CAPTAIN will investigate two important issues specifically for LBNF. The first will be studying low energy neutrinos, which has not been done with a LAr detector. A low energy neutrino source from Fermilab's NuMI beam will be used. Neutrinos detected from a supernova would be in this energy regime. In a separate phase of the experiment, neutron data from CAPTAIN will provide a better understanding of backgrounds for supernova neutrino measurements. The second important task is studying medium energy neutrinos produced in a long baseline neutrino beam. Neutrinos in a long baseline beam can actually change favor (electron, muon, or tau) over a large distance, a phenomenon known as neutrino oscillations [5]. Neutron data from CAPTAIN will be used to better understand interactions that look like electron neutrino appearance events. Furthermore, CAPTAIN will be an important tool in studying CP violation and developing techniques for neutron counting and energy reconstruction.

The CAPTIN detector is still under construction, including the TPC. A group at the University of California Irvine is responsible for making the four hexagonal wire planes that will be used as the grid, U, V, and anode planes. Data from the TPC planes allow for particle detection and track reconstruction. For CAPTAIN each wire plane contains 667 wires, and so there are nearly 2,700 wires in total that need to be soldered and glued to the frames. Construction is expected to begin in the summer of 2015 at UCI's High Bay Facility. Once completed, the wire planes will be transported to LANL and integrated into the master TPC assembly.

1.3 The Prototype for CAPTAIN: mini-CAPTAIN

The prototype for CAPTAIN is appropriately named mini-CAPTAIN, which uses $1/12^{th}$ as much instrumented liquid argon and has half as many TPC wires [4]. A prototype detector allows for testing of the electronics system in cold conditions and testing of the back-end data acquisition (DAQ) system. Moreover, analysis and calibration techniques can be developed while commissioning mini-CAPTAIN. The commissioning phase for CAPTAIN will therefore be faster, and improvements can be made in light of everything learned from the prototype. Therefore, the mini-CAPTAIN detector serves as an important step in realizing the full potential of CAPTAIN.

A crucial aspect of any LAr detector is maintaining a high level of liquid argon purity. To achieve this in mini-CAPTAIN, a filtration system has been implemented by Walter Sondheim and tested by Qiuguang Liu, who are CAPTAIN collaborators from LANL. The purity of liquid argon is enhanced and monitored by the inline filtration system. A further

enhancement to mini-CAPTAIN was made in April 2015, when the condensing system was successfully implemented and tested. The condenser is part of the recirculation system, as it cools the evaporated argon gas back into a liquid using liquid nitrogen at lower temperature. A member of the collaboration, Dr. Hanguo Wang from UCLA, designed this system. He also provided the cryostat for mini-CAPTAIN.

The original schedule for commissioning mini-CAPTAIN was the end of 2014; however, issues with electronic noise and purity have obscured signals in the TPC data. While important progress has been made with the photon detection and condenser systems, a full muon track has not been reconstructed with the TPC data (as of May 2015). Problems with power-source noise and electronic noise washed out cosmic muon signals on the TPC wires for the first several runs, and so it has been difficult to identify a signal amongst all the high and low frequency noise. Lower than expected LAr purity also contributes to the difficulty of finding a muon track. Lower purity means shorter drift distances of the ionized charge, and hence fewer wires (if any) are hit. With improvements made to lower noise and heighten purity, along with analysis software tools that have been developed, the collaboration is expecting to see a muon track through the TPC after the next argon fill during the summer of 2015.

My contribution to mini-CAPTAIN is in the muon telescope data analysis (see chapter 2), placement of the telescope (ch. 3), analysis of TPC data (ch. 4), and correlating events between the two detector systems (ch. 4). Additionally, I will be helping with construct of the TPC for CAPTAIN with a group at the University of California Irvine. The UCI group is lead by Michael Smy and Jeff Griskevich. Construction of the TPC will involve gluing and soldering 667 wires across each of the four hexagonal TPC wire planes, a

process done on independent, movable frames. Upon completion, the wire planes will be transported and integrated into the TPC assembly at LANL. A picture of a mini-CAPTAIN TPC wire plane constructed at LANL is shown in figure 1.2. The planes for CAPTAIN, however, have twice the apothem and thus present further engineering challenges.

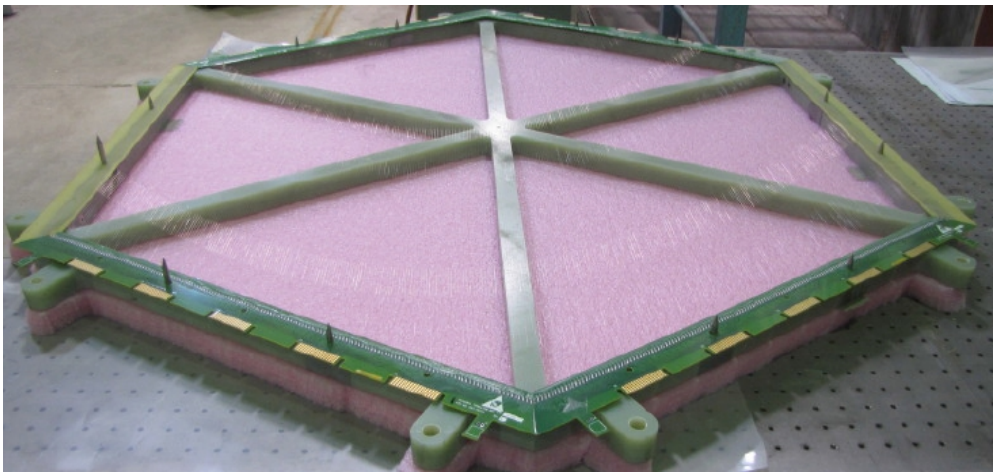

Figure 1.2 – TPC Wire Plane for mini-CAPTAIN

1.4 The Liquid Argon Time Projection Chamber

The time projection chamber was invented in the mid-1970s and soon became an indispensable tool in particle physics experiments. Unlike previous detectors, which could only reconstruct particle tracks in one dimension, a full three-dimensional track can be found with a TPC [6]. Besides giving better resolution for a track, this also allows for a much greater number of tracks to be accurately reconstructed simultaneously. A detection volume is filled with a liquid or gas that can be ionized, and a high voltage is held across the volume. When a charged particle passes through the TPC, it ionizes the medium along its path [7]. The electrons kicked off by the particle are pulled to one side of the TPC by the

applied electric potential. While drifting through the detection volume, charge passes by a series of wire planes that sit perpendicular to the drift direction. The electron drift trajectory is straight, which is very advantageous for tracking electrons compared to the curved trajectories in earlier types of particle detectors.

For CAPTAIN there are two induction planes that take data, called the U and V planes, and these wires are held at a high bias voltage. A third induction plane (the grid plane) is not connected to any electronics, but rather is used to sandwich the U plane. A bipolar signal is induced on the induction plane wires. At the end of the detection volume, the drifting charge is collected on the anode plane (note that this is actually positive charge collection). The U, V, and anode planes are rotated at 60 degrees with respect to each other, as shown later in figure 4.5. Having a hexagonal shape for the wire planes makes sense, as the three planes completely overlap with each other and nicely stack together.

Initially, TPCs were filled with a gas, such as argon. Using liquid argon instead of the gaseous form means there are more particle interactions since the medium is more dense. This is particularly beneficial in neutrino experiments. With the success of ICARUS in the 80s and 90s, the LAr TPC became a frequently used type of particle detector. The LAr TPC combines the resolution capability of older bubble chambers with the advantages of having data that can be converted to digital signal. A cryostat is used to house the TPC and keep the argon below it's boiling point. Even still, the argon continuously boils off, and so refilling is an ongoing necessity. For mini-CAPTAIN the LAr level drops roughly 5 cm every day [8].

A liquid argon detector is ideal for use in long-baseline neutrino oscillation experiments. Such detectors, like the one used for DUNE, allow for the investigation of measuring neutrino oscillation mixing angles, CP violation, the neutrino mass hierarchy,

and interactions of neutrinos that go beyond the Standard Model of particle physics. Functionally, a LAr TPC can achieve millimeter precision tracking and total absorption calorimetry. It can also be used for nucleon decay searches and making cross-section measurements for understanding interaction backgrounds that are important for neutrino experiments. The latter is one of the main goals of CAPTAIN.

There are some difficulties, however, with this type of detector. The trend in neutrino physics has been to increase detector volume. A larger detector has the benefit of seeing more events because there is more material for neutrinos to interact with. Liquid argon, however, does not allow for long electron drift distances unless the purity is extremely high. For CAPTAIN and mini-CAPTAIN the vertical drift distance is 100 cm and 32 cm, respectively. A voltage of 500 V/cm is applied in CAPTAIN and mini-CAPTAIN. An oxygen level of 10 parts per billion or less is required to just obtain a 1 cm drift distance [8]. The contaminant O_2 molecules will grab the drifting electrons, hence attenuating the signal.

Besides dealing with low purity issues, another common difficulty with LAr TPCs is having noisy wires. High electronic noise can be larger than the signal itself, which makes the task of finding wires hit by particles nearly impossible. Unfortunately, electronic noise was especially problematic for mini-CAPTAIN. There were multiple sources of noise, including one of the power supplies and occasional static discharge. A third problem with TPCs is that wires occasionally go dead. If many wires are dead in a localized area, then there is a problem. Having a couple dead wires spread out over the plane, however, does not significantly reduce the tracking resolution or the chance of reconstructing a track. In any case, a periodic check must be performed that all electronic channels are still working.

1.5 Scintillators

Scintillators play a small but important role in mini-CAPTAIN, specifically in the muon telescope (see section 2.1 for a discussion on the telescope). Data is written from the muon telescope to the DAQ when charged particles pass through scintillator paddles located in the center of the telescope wire planes. An incoming particle excites the material in the scintillator paddles, and the material emits the absorbed energy in the form of light [9], which is easily detectable. The scintillator paddles on the telescope therefore provide a reliable cosmic muon triggering mechanism. Multiple scintillator paddles can be used to give stricter requirements for triggering. For example, in the initial runs for mini-CAPTAIN a paddle is placed in front of telescope planes on both sides of the cryostat. Requiring both paddles to scintillate means that most or all data written should contain muon events that passed through the cryostat (and hopefully through the detection volume).

CHAPTER 2: MUON TELESCOPE DATA ANALYSIS

2.1 Muon Telescope Geometry and Layout

The muon telescope is a series of wire planes that are contained in gas-filled chambers, each known as a multi-wire chamber. A charged particle passing through the chamber will ionize the gas, and the generated ionic charge drifts to the nearest wire. Between each wire a voltage difference is applied, thereby making little drift cells within neighboring wires. At the end of a plane a long, coiled wire called the delay line connects every wire. Collected charge travels to the delay line and then to both ends of the line. In mini-CAPTAIN the multi-wire chambers are used to reconstruct cosmic muon tracks, and hence the detector system is named the muon telescope.

Each plane in the telescope contains 75 wires spaced out by 8 mm, where all wires are parallel and lie in a plane. Let W be defined as the wire spacing ($W \equiv 8$ mm). Half of the planes have horizontally spaced wires, called type-X planes. Those with vertically spaced wires are called type-Y. This naming convention follows from the chosen telescope coordinate system, where the y-axis points up and the x-axis points horizontally along the face of the wire planes. Note that the two types of planes are identical to each other, just rotated by 90 degrees.

Figure 2.1 shows a type-X and type-Y plane with a delay line attached to the bottom of the type-X (the delay line for the type-Y plane is omitted). At each end of the delay line, the charge arrival time is clocked by timers A and B. The raw timing data from type-X and type-Y planes is used to determine the x-position and y-position of a hit, respectively. See section 2.2 for the conversion of raw data into a physical position.

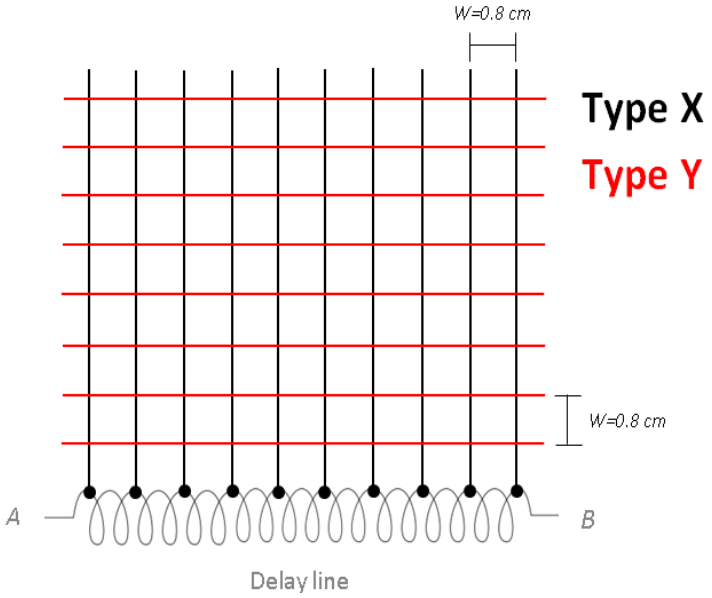

Figure 2.1 – Wire Planes with Delay Line

If only one wire plane is used, it is impossible to know whether the particle passed on the left or right side of a hit wire. To break this ambiguity, two planes of the same type are placed consecutively, offset by half a wire spacing (see figure 2.2).

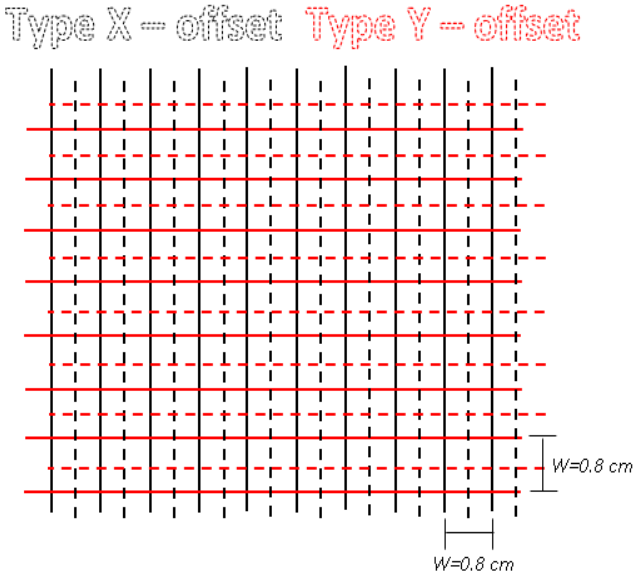

Figure 2.2 – A Muon Telescope Wire Chamber

Figure 2.2 represents a wire chamber, which is defined as two type-X planes and two type-Y planes. Consecutive, offset planes of the same type allows for better particle tracking. Determining which side of the wire the particle passed on allows one to know whether the drift distance should be added or subtracted from the hit position. This improves precision of tracking in the *x* and *y* directions for type-X and type-Y planes.

Each wire chamber is contained in its own frame; therefore, it is possible to move around the four wire chambers independently to optimize muon tracking. For a discussion on the ideal positioning of the muon telescope see section 3.2. For details on how the final configuration of the telescope chambers changes, see section 3.4.

For the initial data runs, all four wire chambers are used. The mini-CAPTAIN cryostat was first filled at the beginning of October 2014. Two wire chambers were placed on opposite sides of the cryostat. All chambers were positioned perpendicular to the ground. Figure 2.3 shows the configuration of the wire planes during the October runs, with the cryostat in the center and two chambers on opposite sides.

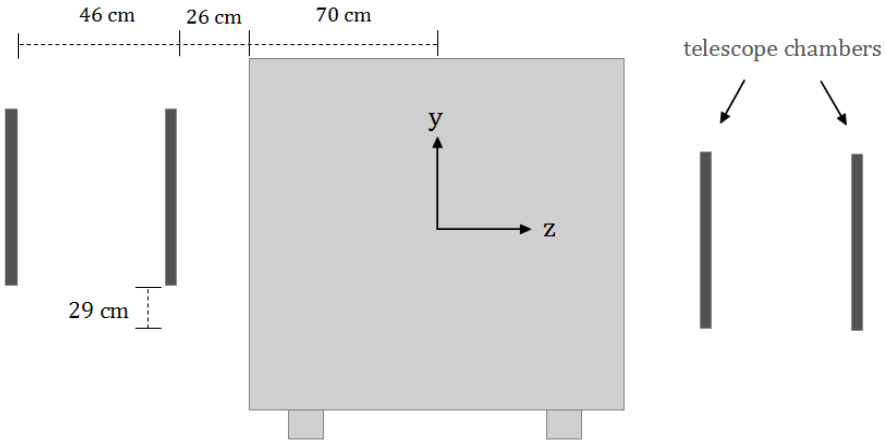

Figure 2.3 – Telescope Chambers and Cryostat Configuration

The muon telescope coordinate origin is located roughly at the center of the cryostat. Note the eight planes on the left side are higher up than those on the right side. The reason for doing this is to track downward cosmic muons that are traveling left to right in the figure. Downward tracks from right to left are also seen in the data but are much less common.

As mentioned, figure 2.3 shows the telescope chamber configuration for the first data run. It was determined, however, that using chambers only on the right side would be sufficient for tracking purposes. The two right chambers were disconnected on August 20th of 2014. This also cuts down on hadronic showers that contaminated data for the downstream wire planes. Another advantage is that requiring a correlated trigger between planes on both side of the cryostat gives a lower event rate than using just half of the planes.

2.2 Raw Data of Muon Telescope

Raw data from the muon telescope is written to a ROOT file by the DAQ (data acquisition) system. Each ROOT file contains 100 events, as the DAQ automatically creates a new file after the event number limit. Information written to the ROOT file includes the event number, number of hits per event, and a control flag that evaluates the quality of the GPS information. The data files also contain the timing information for both channels A and B for each plane's delay line. In the analysis it is required that both channels are hit so that the time difference can be calculated. This time difference is converted into a wire number and physical position (see section 2.3).

The ROOT files also contains GPS information for each event. The raw GPS information is given as years since 1996, days into the year, number of seconds into the day, and number of nanoseconds into the second. I convert this information into a conventional time and date to be verified against run times in the collaboration's elog. The GPS information is crucial for matching telescope event times to TPC events (see section 4.3).

As will be demonstrated, the telescope data is used to find muon tracks that have intersected the wire planes in the TPC. This allows for the signal on a TPC wire to be verified as an actual hit from a cosmic muon track rather than electronic noise. The first step of the analysis is to fit the data to a straight track.

2.3 Fitting Telescope Data to a Linear Track

Let t_A be the arrival time of charge for channel A of the delay line (and similarly t_B for channel B). The difference of the arrival time of charge between channels A and B is then defined as $\Delta t \equiv t_A - t_B$. Note that $\Delta t = 0$ means the center wire is hit, as charge would have arrived to both ends of the delay at the same time. The unit of Δt is TDC (time-to-digital-conversion) counts, and the conversion to seconds is by a trivial calibration factor that need not be used for the purpose of my calculations.

A histogram of Δt values for one particular wire plane (number 7) is shown in figure 2.4, where the horizontal axis is TDC counts. There are clear peaks in the histogram with each peak corresponding to a wire. The largest peak is found in the center because the scintillator paddles that trigger the DAQ to write data are in the middle of the telescope planes. Muons passing along the outside of the planes are unlikely to be triggered on, and

hence they are not well-represented in the data. As shown in the upper-right of the figure, this plot is an accumulation of nearly 9,000 wire hits on plane 7.

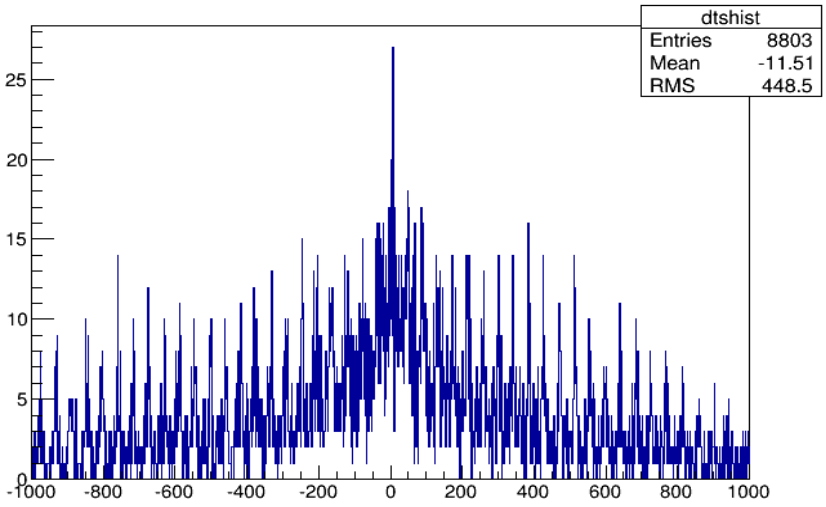

Figure 2.4 – Histogram of Δt for Plane 7

Before proceeding to fitting the data to straight track, a number of variables must be defined. Let the distance of the hit position with respect to the center of the wire plane be defined in eqn 2.1 [10].

$$d \equiv a_0 + a_1 \Delta t + a_2 \Delta t^2 \tag{2.1}$$

While the quadratic term seems out of place, it accounts for dispersion caused by a long delay line. This turns out to be a small correction. After determining the position d, the wire number can be found. Let the wire number be defined as k.

$$k \equiv \text{Int}(d/W) \tag{2.2}$$

The integer function Int rounds to the nearest integer. Notice that k = 0 is the center wire, and the range of k is from -37 to +37. From the previous section recall that W is the wire spacing of 8 mm.

A minimization procedure is then used to find the fit constants a_0, a_1, and a_2. Since subsequent wire planes are offset, the value of a_0 differs per plane. This term represents where the center wire is located. The term a_1 is a measure of the wire spacing. In principle, all planes should have nearly identical values for a_1 and a_2. Let the function to minimize for each plane be defined in eqn 2.3 [10]. Note that the index i has a maximum range equal to the number of data points (wire hits) for each plane.

$$\chi^2 \equiv \sum_i (d_i - k_i)^2 \tag{2.3}$$

$$d_i = a_0 + a_1 \Delta t_i + a_2 \Delta t_i^2 \quad , \; k_i \equiv \text{Int}(d_i/W) \tag{2.4}$$

There are three independent ways to perform the minimization calculation and find the fit constants (a_0, a_1, a_2) for each plane. First, I used a native ROOT package known as Minuit. One provides the function, minimization parameters, and initial guesses for these parameters. While this method works in principle, I found the process to be overly sensitive to initial guesses. Consequently, the fit parameters could be drastically different by changing the initial guess by a fractionally tiny amount. Additionally, Minuit did not always give physically reasonable values for the fit constants.

A second way to find the constants is to calculate the peak spacing and center peak location directly by examining the histograms. The best method, however, is to perform a scan over parameter space. A minimum and maximum range for each fit parameter is chosen based on physically reasonable values, and a very small increment is specified to modify each constant. The minimization function is computed for every value of each constant, and the values of the constants that minimize eqn 2.3 are found. While this method can take billions of iterations to perform, a physically reasonable fit is found each time and hence is the preferred method.

Figure 2.5 shows the histogram from figure 2.4 superimposed with solutions of Δt in the following equation. In eqn 2.5 n represents the wire number.

$$a_0 + a_1 \Delta t + a_2 \Delta t^2 = nW \quad , \; n = 0, \pm 1, \pm 2... \tag{2.5}$$

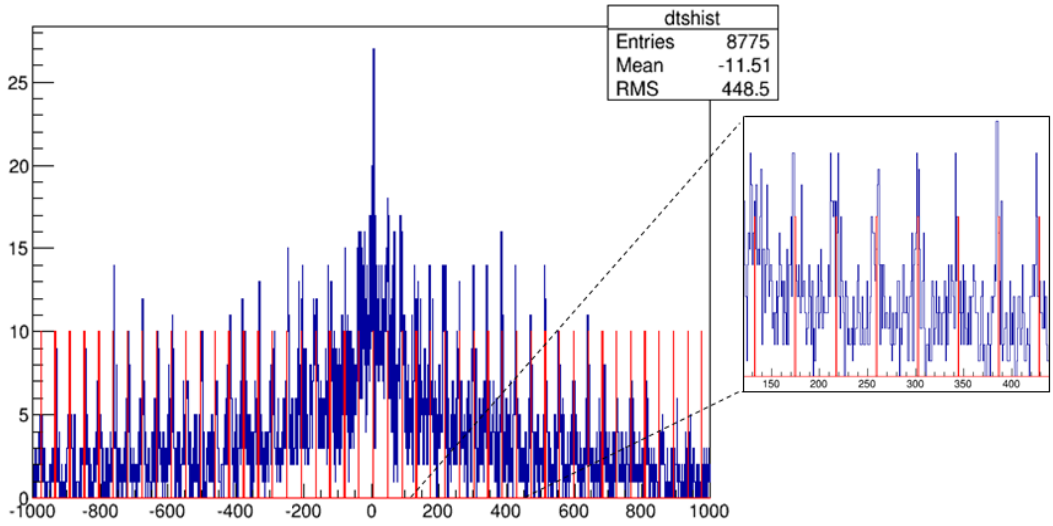

Figure 2.5 – Δt Raw Data with Solutions of Eqn 2.5

The values for the fit constants are calculated to be a_0 = -0.1 cm, a_1 = 0.019 cm, and a_2 = 10^{-7} cm. Note the time units are omitted from these constants. Also notice the quadratic term is a small correction as expected. To improve the quality of the fit, only raw data in the range -600 to +600 is used. It may not be easy to tell from figure 2.4, but the raw data tends to become more spread out and less clustered around peaks outside of this range. Using only the middle section of data means having better defined peaks, which improves the fit.

To check the quality of the fit and the legitimacy of the reconstructed position of wire hits, consider the left histogram in figure 2.6. This is a histogram of the non-squared terms of the chi function i.e. d_i - k_i. The symmetry of the histogram and the peak around zero indicate a good fit for the parameters a_0, a_1, and a_2. On the right side of figure 2.6 is a

plot of the reconstructed hit position i.e. $k_i \cdot W$. Most hit positions are in the center of the plane, which makes sense considering that the scintillator paddle that triggers the telescope is positioned in the center of the wire planes. These are again examples using data from plane number 7.

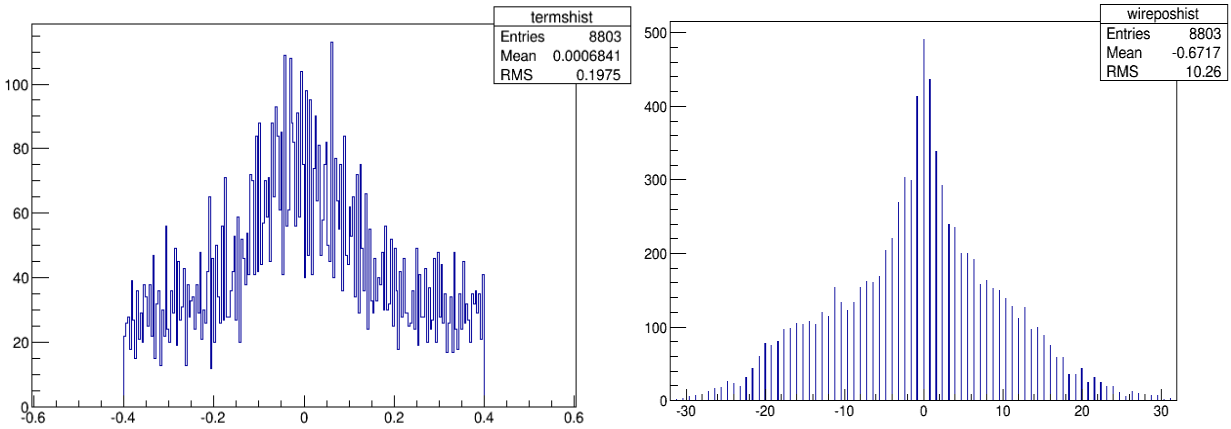

Figure 2.6 – Residuals of Raw Data and Fit Position (left)

Reconstructed Position of Wire Hits (right)

With confidence in the fitting procedure and with good results for plane 7, telescope data for all eight planes is analyzed. Since half of the wire planes are not used after August 20th of 2014, I only consider the remaining eight planes for the remainder of this paper.

In table 2.1 the fit constants for all eight telescope wire planes are given. Again the units of time are in TDC counts but are intentionally omitted. For three of the planes (numbers 1, 4, and 5) the value of a_2 is found to be zero, or at least it is so small that it can be ignored. In my numbering convention, plane 1 is closest to the right side of the cryostat in figure 2.3, and plane 8 is the right-most plane.

Plane Number	Plane Type	a_0 [cm]	a_1 [cm]	a_2 [cm]
1	X	0.005	0.0191	0
2	X	-0.250	0.0179	-9.5×10^{-6}
3	Y	-0.035	0.0183	8.6×10^{-6}
4	Y	0.045	0.0189	0
5	X	0.005	0.0191	0
6	X	0.250	0.0179	-9.5×10^{-6}
7	Y	-0.100	0.0188	1.0×10^{-7}
8	Y	0.045	0.0175	-9.4×10^{-6}

Table 2.1 – Values of Fit Constants

After all the fit constants for all planes have been calculated, a given value of Δt can be converted into a wire number and physical position. If at least three planes of each type (type-X and type-Y) are hit, then a linear fit in the *x*-*z* and *y*-*z* coordinates is performed. Technically, only two points are needed to determine a line, but requiring three points to fit ensures consistently better results. Stray hits from other muons or poorly reconstructed positions can ruin the fit track, and so using only two points is a bit risky. Since there is a sufficient volume of data, requiring three hits of each type is always enforced.

Let the linear fit parameters be *A*, *B*, *C*, and *D* in the following equations.

$$x(z) = Az + B \tag{2.6}$$

$$y(z) = Cz + D \tag{2.7}$$

A more useful form than the linear equations above is a 3D vector form:

$$\vec{R} = \vec{R}_0 + \vec{V}\,t \tag{2.8}$$

$$\vec{R} = (x, y, z) \quad , \quad \vec{R}_0 = (x_0, y_0, z_0) \quad , \quad \vec{V} = (v_x, v_y, v_z)$$

I choose to define the vertex coordinate z_0 and velocity component v_z.

$$z_0 \equiv 0 \quad \text{and} \quad v_z \equiv \frac{1}{\sqrt{A^2+C^2+1}} \tag{2.9}$$

With these definitions for z_0 and v_z, as well as using eqn 2.6 and 2.7 for x and y, the vectors in eqn 2.8 can be written as

$$\vec{R}=(Az+B, Cz+D, z) \quad , \quad \vec{R}_0=(B, D, 0) \quad , \quad \vec{V}=\frac{(A, C, 1)}{\sqrt{A^2+C^2+1}} \tag{2.10}$$

Noting equations 2.6 and 2.7, the type-X hits and type-Y hits provide a series of points to perform a linear fit. The raw data at each plane only gives (x, z) or (y, z) information, where the z coordinate comes from the plane spacing. To acually draw a hit in 3D coordinates (as is done in the next section), the missing piece of information is aquired from the fit line itself. For example, plane 1 gives a point at (x_1, z_1), and the coordinate y_1 is calculated by equation 2.7 using z_1 and the fit parameters C and D. The point (x_1, y_1, z_1) can then be drawn as the hit position for plane 1.

After acquiring the hit positions and fitting them to a straight line, the most important aspect of the data analysis can finally be performed. Recall that the muon telescope can be used to verify signals on TPC wires as muon hits rather than just being noise. Knowing where the muons should have passed through the TPC also enables targeted searching for signals amongst the copious amounts of TPC data. Finding the muon tracks that pass through the TPC volume and calculating which TPC wires should be hit is therefore the main goal of telescope data analysis. This procedure is detailed in section 4.4

2.4 Event Display for Telescope Data

After finding the hit wires and fitting hit position information to a track, it would be nice to verify the procedure thus far. One way to do this is to create an event display. The mini-CAPTAIN collaboration did not have an event display for the muon telescope, so I wanted to make one. The event display draws the telescope planes and hits, the TPC, and the muon track all using native ROOT functions.

An event display allows for a visual verification that the analysis procedure gives a reasonable looking fit track. One can also easily seen whether that track appears to pass through the TPC or not. Figure 2.7 shows an example track that passes through the top face of the TPC and exits the back vertical face. At the center of figure 2.7 is the hexagonal TPC, but the cryostat is not drawn in the event display.

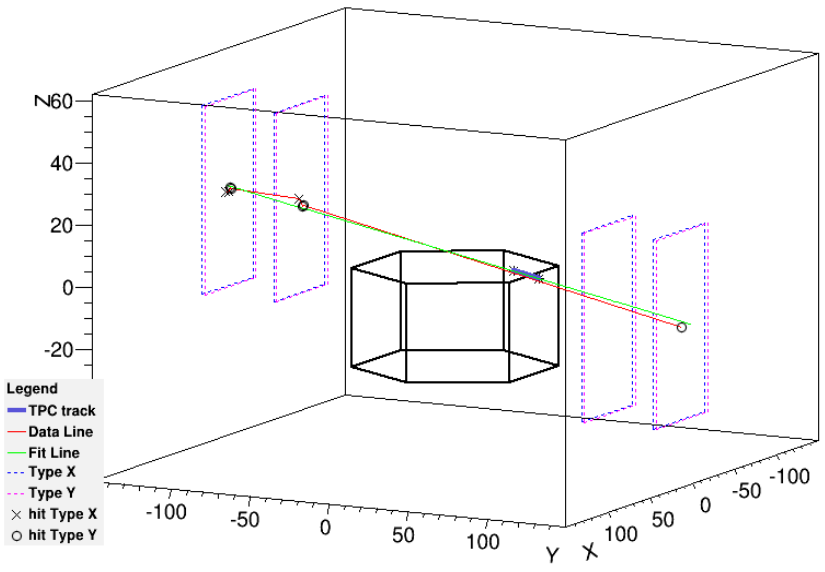

Figure 2.7 – Event Display of a Telescope Event

As seen in the legend at the bottom-left of 2.7, the segment of the fit track that passes through the TPC is a thicker blue line; the line connecting all data points is red; the fit track is green; and the markers represent the location of type-X and type-Y hits. Note that the axes have units of centimeters. Each telescope plane drawn actually represents two planes of the same type.

An important remark about the event display is that it is drawn in TPC coordinates, not in telescope coordinates. The top face of the TPC defines the $z = 0$ plane, and the center of the top face is origin $(x', y', z') = (0, 0, 0)$. Primed coordinates will be used to represent the TPC coordinates system. The linear fit of telescope hits is always performed in telescope coordinates for simplicity, and then the hit locations and fit track are transformed and drawn in TPC coordinates. As will become apparent in chapter 4, the calculations are much simpler by converting telescope information into the TPC picture and not the other way around.

A fair amount of work is required to figure out if the muon track intersects the TPC and exactly where the intersection occurs. In short, a check is performed for all eight faces of the TPC individually. Four of the faces are defined as entry faces, and the other four are exit faces. To this end, a TPC track is found when one entry face and one exit face is intersected. I thoroughly tested this code by looking at many events that go through various combinations of entry and exit faces.

Other views of the event display can be useful, such as a side view and top view, as shown in figure 2.8. These are automatically generated on separate ROOT canvases for convenience. In this way, the code can be used to easily monitor real time data and help understand where exactly the fit track enters and exits the TPC. I hope to pass on my

analysis and event display code to a collaborator at LANL for integration into the DAQ system for real-time telescope data monitoring.

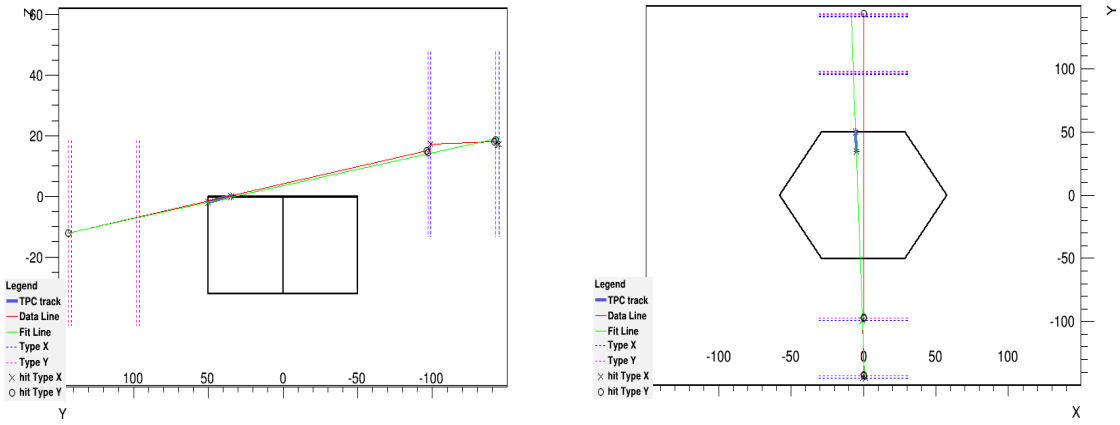

Figure 2.8 – Side and Top Views of the Event Display

Since the telescope data fit tracks and hit positions look reasonable, the next and last step of telescope data analysis is to characterize the tracking errors. I need to understand the uncertainty of the muon's location at each TPC wire plane, particularly in the direction perpendicular to the wires. This is required to understand the accuracy of my list of TPC wires that should have been hit by the muon event (see section 4.5 for a detailing of this process).

CHAPTER 3: POSITIONING OF THE MUON TELESCOPE

3.1 Angular Studies of Telescope Data

It was originally desired to see horizontal muon tracks through the TPC, hence the configuration shown in figure 2.3. Near-horizontal tracks create a long track of ionized charge that will drift up to hit most TPC wires, whereas near-vertical tracks may only hit a few wires. Due to the relatively low rate of telescope events that pass through the TPC, the mini-CAPTAIN collaboration decided to change the telescope's configuration. Getting a higher fraction of telescope events that pass through the TPC can be achieved by moving and titling the telescope planes to increase cosmic muon flux.

Before proceeding to optimize the telescope's configuration, I want to characterize the data from the initial setup. First, I study the angular properties of telescope fit tracks. Consider the zenith angle of tracks as measured from the positive z' axis. Data from October 9^{th} to 16^{th} is analyzed, in which only eight telescope planes were used. Looking over 17,911 events from the October data, the zenith angle θ is plotted in units of degrees in figure 3.1. Only events that hit at least six telescope plane hits are considered.

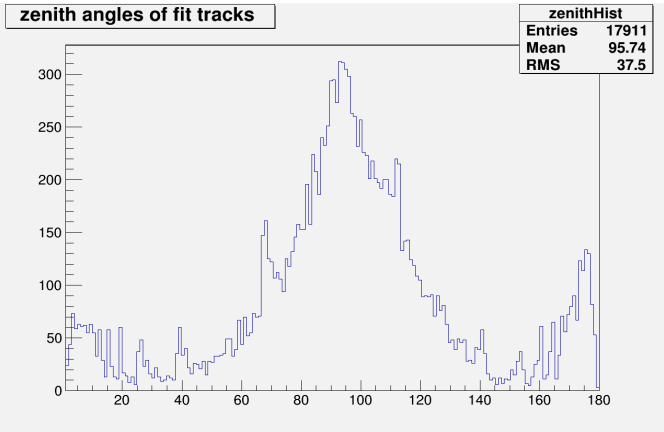

Figure 3.1 – Zenith Angle of Fit Tracks

In light of the vertical orientation of the telescope planes, it is expected that most tracks through the telescope are near-horizontal. In figure 3.1 there is a clear peak around 90 degrees. Smaller peaks are also seen around 0 and 180 degrees, which corresponds to near-vertical cosmic muons. The flux of near-vertical cosmic muons is very high, so it makes sense this has a strong presence in the data, even if the setup is biased for near-horizontal tracks.

A phase-space correction can be made by re-weighting the histogram by the integral of the solid angle over each histogram bin (with a bin width of one degree). Figure 3.2 is re-weighted by this correction, which changes the overall shape as seen in figure 3.2. After the correction, the histogram has a closer resemblance the actual cosmic muon distribution of $\cos^2(\theta)$. A local maximum is still present around 90 degrees.

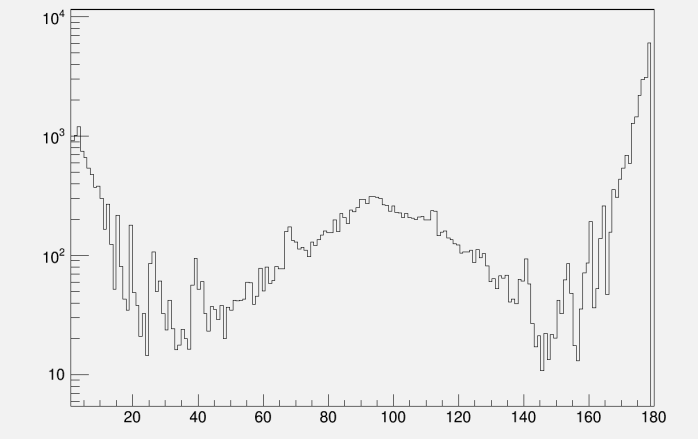

Figure 3.2 – Zenith Angle with Phase-Space Correction

To further characterize the telescope data, I plotted the track residuals i.e. the difference between the position of each wire hit and the location of the fit track at that hit wire's plane. Initially, this was done to check the validity of the fit, as having large differences between the fit positions and hit positions means there will be large tracking

uncertainties. In studying the residuals, however, an important asymmetry between data from type-X and type-Y planes was realized and provided further motivation for relocating the muon telescope.

Figure 3.3 shows logarithmic plots of the tracking residuals for type-X hits (left) and type-Y hits (right). Again this data is from the October runs, and all four type-X planes are combined into one plot, as is the case with type-Y planes. These two plots were generated with the same data set, yet type-X hits only make up about 43% of all recorded hits (noting the number of entries shown in each histogram). Since all eight planes were functioning, this indicates that the data for type-Y planes is contaminated by stray hits from the large flux of near-vertical muons, and so fit constants for these planes may be skewed.

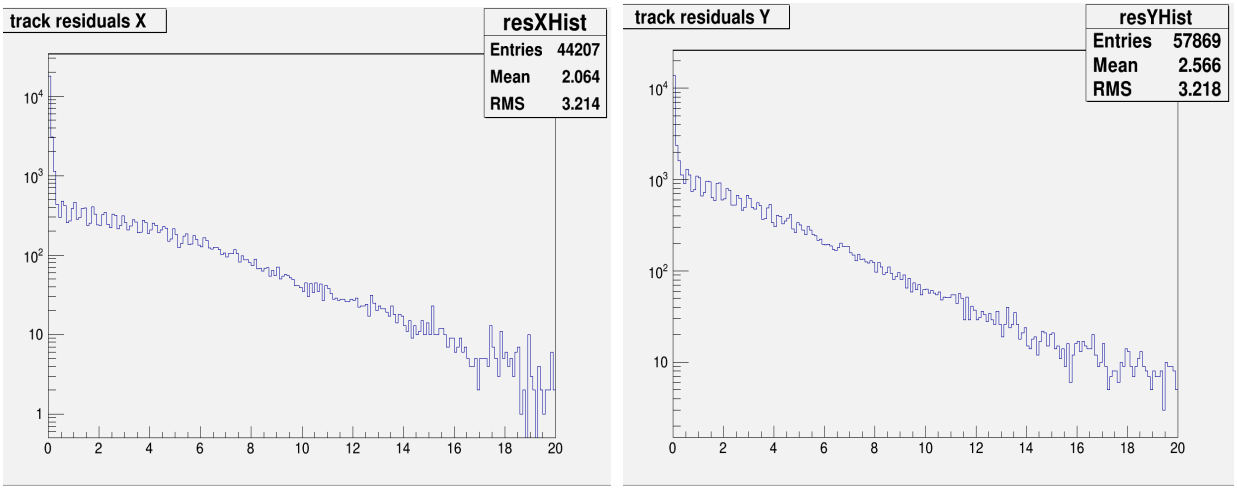

Figure 3.3 – Track Residuals for Type-X (left) and Type-Y (right) Planes

After looking at the angular properties and tracking residuals of the muon telescope data, a few conclusions can be reached. A horizontal telescope plane (with its face parallel to ground) will capture the most cosmic muons, whereas a vertical plane captures the least. Tilting the planes could therefore greatly increase the flux. Not only that, but a much higher

fraction of telescope events would go through the TPC if the planes were in a better location. To obtain better coincidence between the telescope data and TPC data, the muon chambers are repositioned, giving overall more useful data.

3.2 Positioning of Telescope Plane to Maximize Flux

The change in flux for various telescope plane configurations is studied. After changing the plane's location with respect to TPC, the optimal tilt angle can be calculated that maximizes the flux of muons through the telescope plane and the center of the TPC. A contour map of the maximized flux and tilt angles for various locations can then be made.

Consider the geometry of a tilted telescope plane, shown in in figure 3.3. Let L_1 and H_1 be the horizontal and vertical distances from the center of TPC to the right edge of a telescope chamber (labeled as point *P*). Here the origin is defined to represent the TPC's location. For simplicity, it is represented as a point. In figure 3.4 the value of *w* is 0.6 meters, which is the width of a wire chamber (75 wires with 8 mm spacing gives a 0.6 m width).

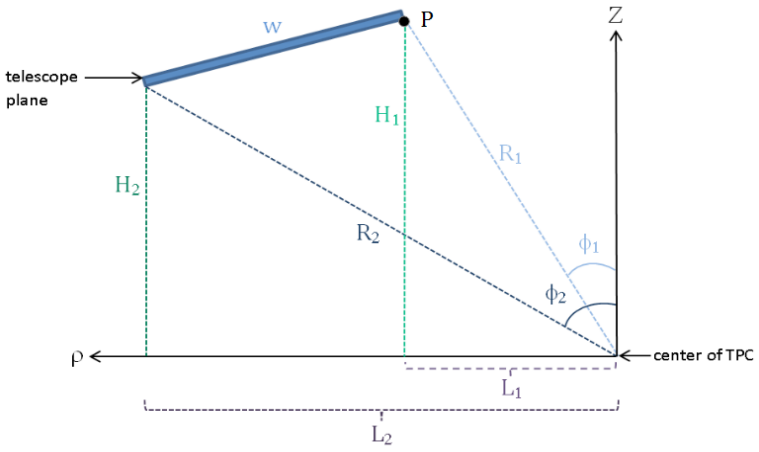

Figure 3.4 – Geometry of Tilted Telescope Plane

The mathematical end-goal is to maximize the integral of cosmic muon flux over the solid angle of a telescope plane for each location. It is convenient to assume the plane is centered about the *x*-axis, as to provide symmetry over the ϕ coordinate. The total angular spread in ϕ at the center of the wire plane is found using the arc length formula.

$$w = \Delta\phi \cdot (L_1 + L_2)/2 \tag{3.1}$$

Using the angular spread at center of the plane along the ρ-axis is an approximation that greatly simplifies the calculation. The range of the θ coordinate is easily seen by examining figure 3.4. The bounds of θ should be also written in terms of the dimensions of *L* and *H*. The desired integral to maximize can now be written as the following.

$$\int_{\theta_1}^{\theta_2}\int_{\phi_1}^{\phi_2} \sin(\phi)\cos^2(\theta)\, d\theta\, d\phi \tag{3.2}$$

where $\theta_1 = \tan^{-1}(L_1/H_1)$, $\theta_2 = \tan^{-1}(L_2/H_2)$

$$\phi_1 = -w/(L_1+L_2),\ \phi_2 = w/(L_1+L_2)$$

For the procedure, a value for L_1 and H_1 is chosen, then the value of L_2 and H_2 that maximizes the given integral is determined. A range of 0 to 2.5 meters is used for L_1 and H_1. The tilt angle of the plane θ_p is then found. These calculations are done in Mathematica, which provides many useful functions. Figure 3.5 shows the definition of the tilt angle θ_p.

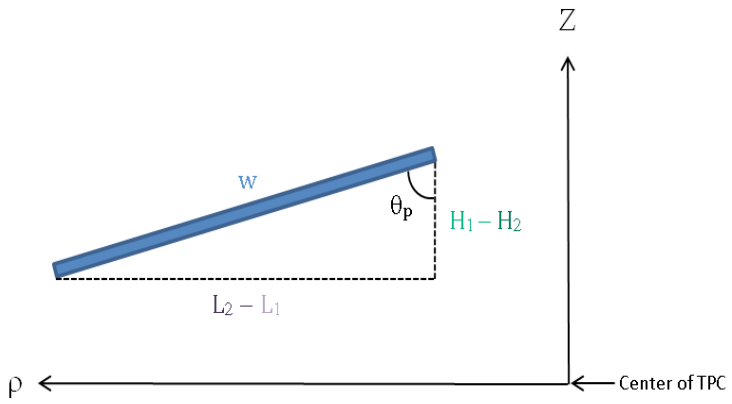

Figure 3.5 – Titled Wire Plane Geometry

Geometric constraints must be determined for the maximization function. For this study it is assumed that the telescope plane remains above the origin, as the planes will be above the TPC in the actual setup. The following geometric constraints are applied:

$$H_1 > H_2 > 0 \tag{3.3}$$

$$L_2 > L_1 > 0 \tag{3.4}$$

$$(H_1 - H_2)^2 + (L_2 - L_1)^2 = w^2 \tag{3.5}$$

To visualize the change in the maximized flux for given locations of the telescope plane, a colored contour is made (see figure 3.6). The horizontal axis represents values of L_1 and the vertical is values of H_1. Colored sections in 3.6 represent different maximum values of cosmic muon flux. White represents locations with the largest possible flux, and light purple represents the lowest.

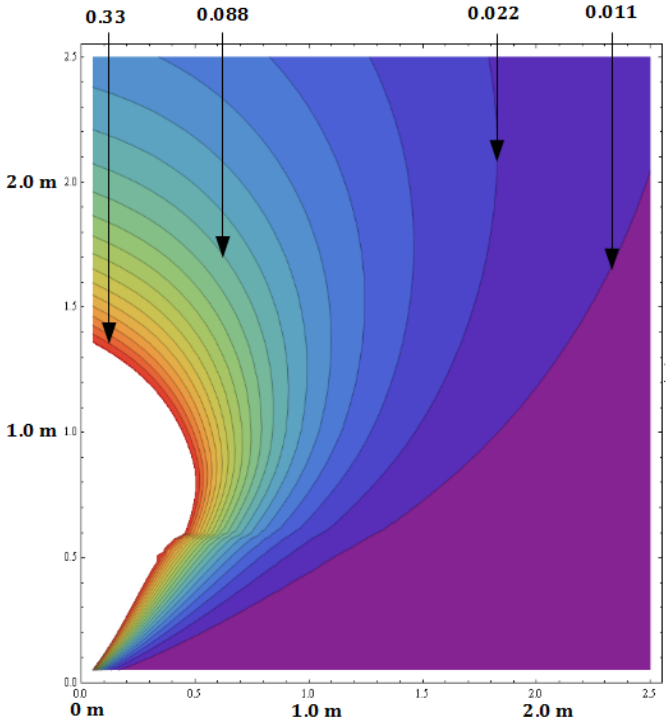

Figure 3.6 – Maximum Flux Contour Map

Contours are labeled with numbers only to show relative values. These numbers must be multiplied by the cosmic muon event rate over the plane area to get the actual flux. Notice there is warping around $H_1 = w = 0.6$ m, which is most prominent in the white through green regions. This is because $H_1 > H_2 > 0$ is enforced as a geometric constraint, so the telescope plane cannot tilt freely when $H_1 < w$, hence the contours are skewed.

It is important to note that the region $L_1 < 0.7$ m is not physically accessible since the cryostat has this radius. Therefore, the optimal location of point P (recall figure 3.4) is

$$(L_1, H_1) = (0.7 \text{ m}, 1.0 \text{ m}).$$

Next, the tilt angle at each location is calculated and plotted in figure 3.7, which maps the value of θ_p at locations of (L_1, H_1). Again the contours are skewed in the region $H_1 < w$ since the bottom edge of the plane cannot tilt any lower than $Z = 0$. The contour labels are in units of degrees, as measured from vertical. The large purple region represents tilt angles below 3.8 degrees. For the optimal location (0.7, 1.0), the tilt angle is roughly 8 degrees.

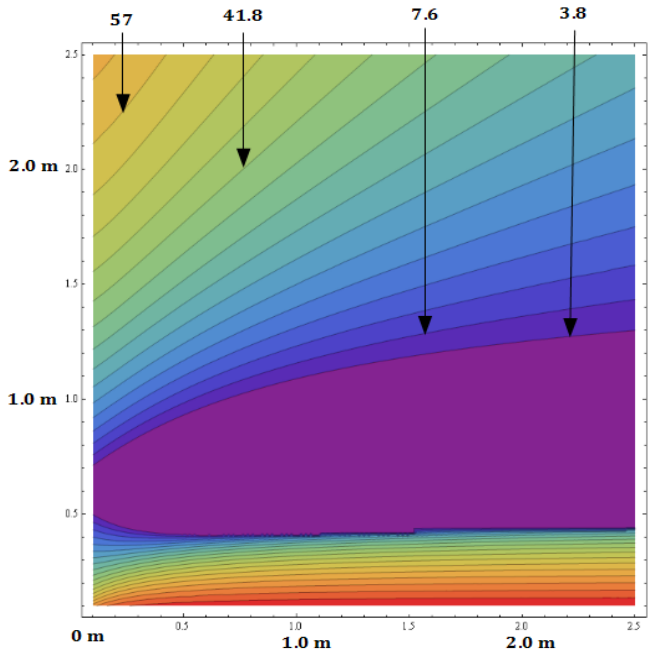

Figure 3.7 – Optimized Tilt Angle Contour Map

3.3 Approximations Used in Previous Section

It is important to understand the limitations of this study. While the results are useful and certainly provide motivation for relocating the telescope planes, this study is not completely rigorous. One approximation used, as already mentioned, is that the TPC is simply represented as a point. This approximation is fine since the main concern is simply increasing the amount of tracks through both the telescope plane and the TPC. Whether the increase is by a factor of two, three, or another number is not necessarily important.

Another approximation is used in the integral bounds over ϕ. The angular spread of the plane width in ϕ varies with its distance along the ρ-axis. More specifically, the top section is closer to the origin than the bottom since the plane is tilted and would therefore have a larger spread in ϕ. Instead of using exact expressions for the integral bounds, which would give rise to a much more complicated integral, the spread in ϕ is assumed to be constant. The integral is therefore over the center of the plane, where the distance to the origin is the average of the closest and farthest edge or $(L_1 + L_2)/2$. This approximation should not significantly change the shape of the contour plots.

Lastly, only one telescope plane is considered. This study could be expanded to include 4 planes in close proximity to represent a wire chamber. Perhaps even multiple wire chambers could have been be used. Adding multiple wire planes in close proximity would not change the results of this study significantly. If I require that all the planes need to be hit by a cosmic muon, then there would just be a slight reduction in flux. Such a complication, however, would necessarily be useful for the study.

3.4 Optimal Location of Telescope and Final Positioning

During the October run the telescope planes sat 26 cm away from the cryostat. Looking at the contour map in figure 3.6, I see that moving the telescope planes 26 cm closer to the TPC and titling the planes gives an increase in the flux by roughly a factor of three. In fact, the "good" events in the October run are separated by 5.54 minutes on average, whereas those in the March run are separated by 1.67 minutes (3.32 times more frequent). I define a "good" event as one that should have at least ten hit TPC wires (see section 4.4). After discussing these finding with the CAPTAIN collaboration, the muon telescope was relocated.

The planes are tilted toward the top of the TPC as to increase data coincidence between the two detector systems with an angle of 45 degrees. In figure 3.8 the new configuration of the muon telescope is shown. This drawing is courtesy of Charles Taylor from Los Alamos National Lab.

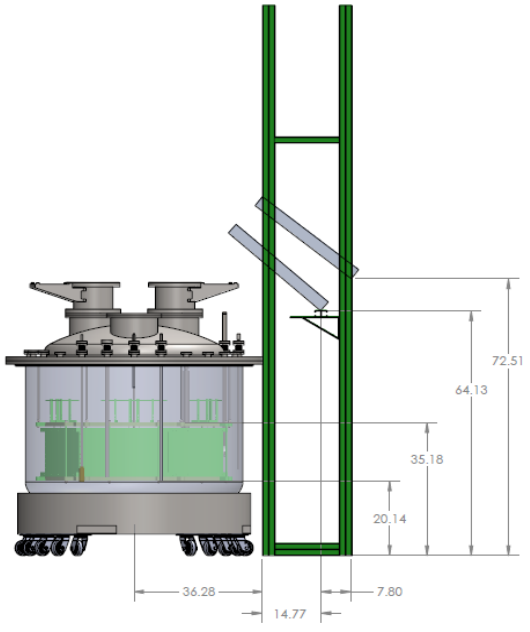

Figure 3.8 – New Position of Muon Telescope

The planes are located as close as possible to the top of the cryostat while avoiding all of the valves, wires, and electronic boards. During the March data runs discussed in the next chapter, the setup shown in figure 3.8 is used. More detailed dimensions of the telescope apparatus is shown in figure 3.9, again provided by Charles Taylor. The physical measurements are a vital aspect of ensuring a proper coordinate transformation in the code and a reliable analysis of the data. In figures 3.8 and 3.9 all dimensions are in inches.

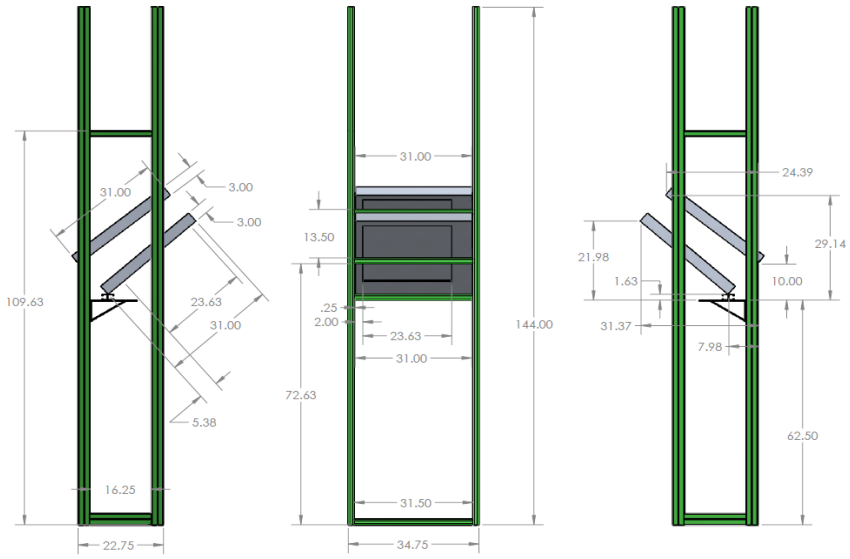

Figure 3.9 – Detailed Geometry of Muon Telescope

New telescope data was taken in February of 2015 after the TPC is refilled with liquid argon. Initially, the data did not look promising, as most if not all of the telescope fit tracks seemed to miss the TPC volume. The location of the scintillator paddles was also a contributing factor for this. After moving the plane closer and higher up, a large fraction of events intersected the TPC volume with an improved event rate compared to data from October. Analyzing the data from March 5th - 8th reveals 1,029 good events among 79,900 total events. Recall that a good event has a track that gives at least ten candidate wires. This

demonstrates that moving the telescope planes has a positive effect on the amount of useful data. The March data run will be discussed in greater detail in the next chapter

A typical muon track with the newer telescope configuration is shown in figure 3.10. All eight telescope wire planes are hit. In this figure the hit telescope wires are also drawn in (section 4.4 details this procedure). The event in figure 3.10 was recorded on March 13th at 18:59:58 Greenwich Mean Time (GMT). Hundreds of TPC wires should have a signal, assuming a sufficiently good liquid argon purity. This ensures that electrons generated toward the bottom of the TPC can drift all the way up to the wire planes.

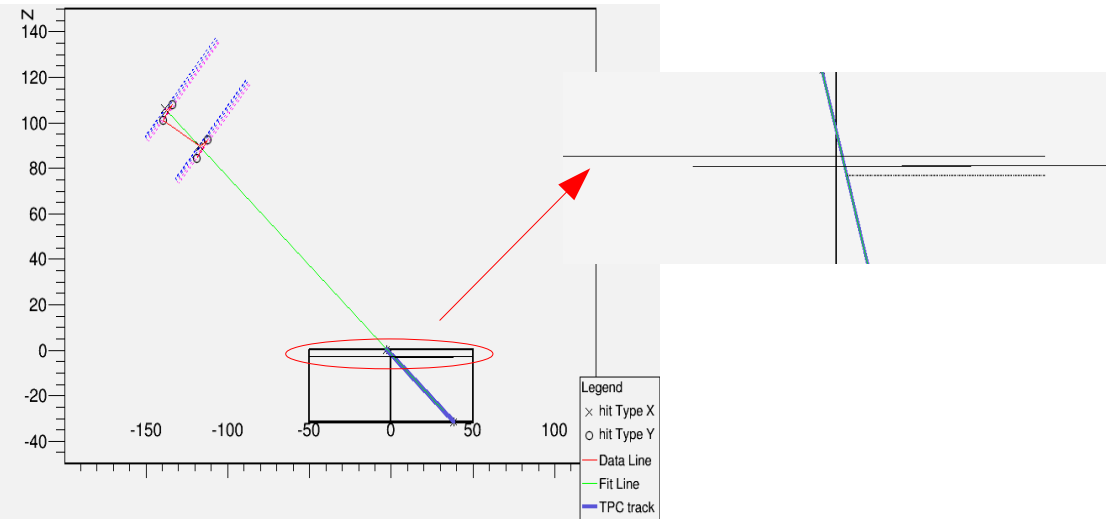

Figure 3.10 – Telescope Track (left), Zoomed View of TPC Planes (right)

The remaining steps are to introduce the TPC geometry, analyze data from the TPC system, calculate the candidate wire list, and finally plot TPC data from the potentially hit wires to find a cosmic muon signal. A discussion on telescope tracking uncertainties is reserved for section 4.5. It is first important to understand the geometry and orientation of the TPC wire planes. Characterizing the uncertainty in the fit track's position at each plane helps to understand the accuracy of the candidate wire list.

CHAPTER 4: TPC DATA ANALYSIS

4.1 TPC Geometry

A drawing of mini-CAPTAIN's TPC is shown in figure 4.1, where all dimensions are in inches. This drawing and figure 4.2 were provided by LANL. The TPC sits in the middle of the cryostat, so it is fully submerged in liquid argon when the cryostat is filled. The green rectangular outline is the TPC's frame, and inside the frame is a large amount of planes with various functions.

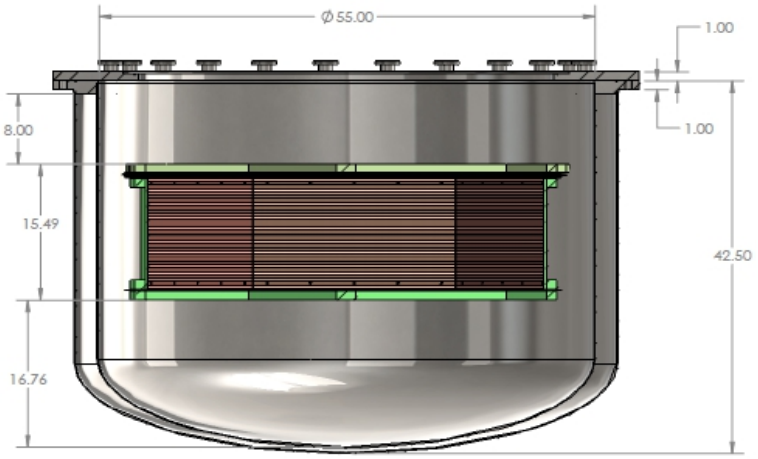

Figure 4.1 – Drawing of mini-CAPTAIN's Cryostat and TPC

Ionic charge is generated by a cosmic muon as it passes through the liquid argon. A voltage difference of 500 V/cm is maintained between the cathode and anode planes, which are toward the bottom and top of the TPC's volume separated by 32 cm [4]. The charge is pulled upward through the TPC toward the anode plane. Charge passing by wires on the induction planes (the U and V planes) induces a bipolar signal. At the anode plane charge is collected, inducing a mono-polar signal.

The three hexagonal wire planes that provide raw data are sitting toward the top of the TPC, separated only by 3.18 mm. From bottom to top, the plane order is grid, U, V, anode, and ground plane plane. The zoomed cross-section view in figure 4.2 is of the upper-left corner of the TPC shown in figure 4.1.

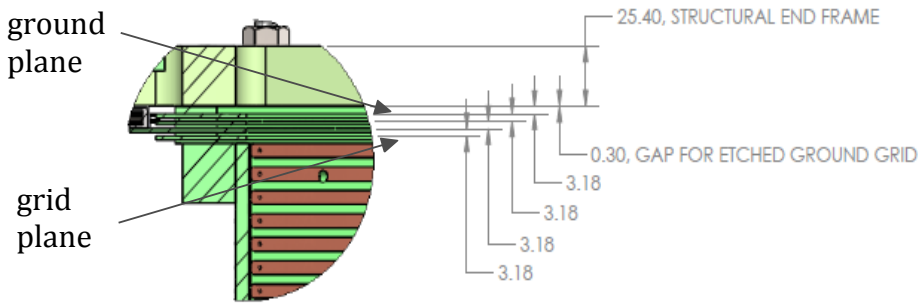

Figure 4.2 – Close View of TPC Wire Planes Spacing

Each of the three active TPC wire planes has 384 electronic channels, giving 1152 channels. In reality, only 319 channels on each plane correspond to active physical wires. Hence there are 957 active wires for the data analysis. Neighboring wires are separated by 3mm. Mapping the electronic channels in the data files to a physical wire is crucial for reconstructing muon tracks from signals found on TPC wires. This track can be compared against the track reconstructed from muon telescope data. In order to make use of the track, there needs to be a way to easily go between the electronic channel picture and the physical wire picture.

A wire mapping table has been made by Charles Taylor. I wrote a program that reads this table and outputs a simple ROOT tree, where the entry number corresponds to the electronic channel and the wire number is the value of each entry. Channels without wires

have a value of 0. While stepping through the TPC data files, a hit channel can be translated to a wire number easily by referencing this ROOT tree.

To translate the wire number into a physical picture, the numbering convention must be understood. For an easy understanding of this convention, I helped create figure 4.3. Each plane contains 335 wires, increasing in number from right to left across the mother boards. The first and last wires are labeled with their number. Not every wire actually takes data, as there are only 957 active wires out of the 1005 wires given in the wire mapping table.

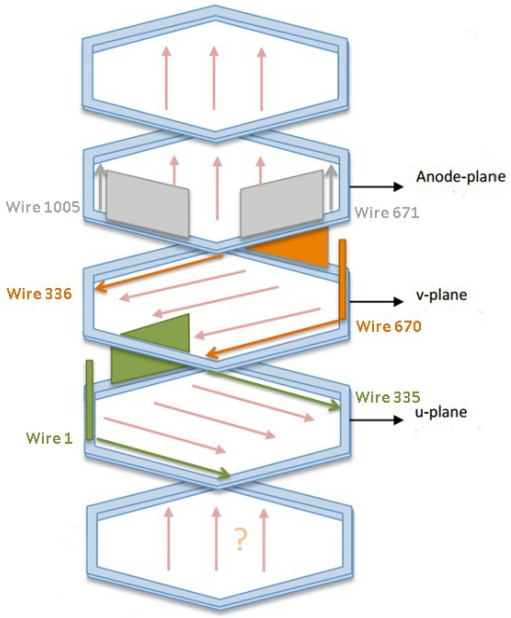

Figure 4.3 – TPC Wire Planes with Wire Number

Now that the layout and wire number of the TPC planes is understood, data from the TPC system can be discussed, analyzed, and compared against the telescope data. A basic program that steps through an ubdaq file was provided by Clark McGrew from Stony Brook University. From this I was able to write a program that compares TPC event time stamps against the GPS information of good telescope events and then plots the relevant raw TPC

data from time-matched events. Before discussing this analysis, I will talk about the TPC's raw data.

4.2 TPC Data – Cosmic Runs and Pulsar Runs

TPC data is written to a special file format, called an ubdaq file. Each event written contains voltage values taken over a 4.8 ms window. The voltage per channel is sampled at 2 MHz (in 500 nanosecond increments) a total of 9,594 times, giving a 4.8 ms window of data per event. Only the middle third (a 1.6 ms interval) of this data is analyzed, called the trigger window.

An ubdaq file can only be read in sequence, meaning there is no random access capability. A consequence of sequenced reading instead of random access reading is that it may take a long time to step through the file to see a particular event of interest. Ubdaq files may contain over 7,000 events. If data from event 7,000 is to be analyzed, then the first 6,999 events must be stepped through. This means going through over 77 billion loops of code:

$$(1152 \text{ channels}) \cdot (9{,}594 \text{ time bins}) \cdot (6{,}999 \text{ events}) = 7.73 \cdot 10^{10} \text{ calculations}$$

There are two different methods of triggering TPC data to be written from wire planes. A function generator can be used to send a pulse at a certain frequency, and this regular pulse triggers the DAQ to write data. A square pulse at a rate of 10 Hz is used. Taking data using this method is called a pulsar-triggered run, or pulsar run for short. A statistical argument motivates taking data with this method: many random muon events

will in inevitably slip into the trigger window if enough data is taken with a high enough frequency.

Instead of using a function generator, the DAQ can be triggered with the muon telescope. These are called cosmic-muon-triggered runs, or simply cosmic runs. For the purpose of correlating telescope events to the TPC events, this method is substantially better. Events are only written to ubdaq files when the muon telescope is triggered, meaning there is a perfect overlap of TPC and telescope data. In pulsar runs, there are almost no events that time-match. One issue that has been seen in cosmic runs is that the muon telescope trigger induces electronic noise on several TPC wires.

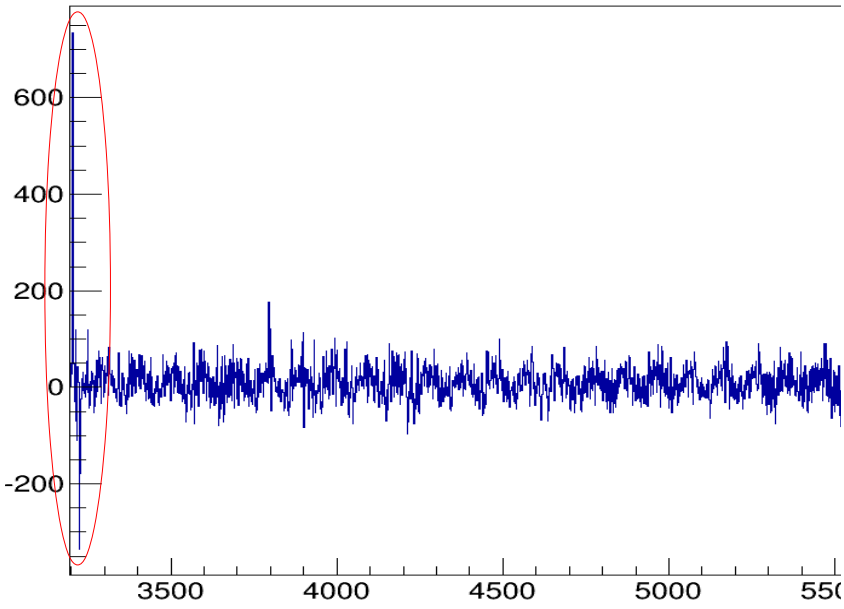

Figure 4.4 – Telescope Trigger Noise on a TPC Wire

As seen in the figure, a large pulse appears at the beginning of the trigger window. It was first thought that this pulse may have been a muon signal. Trigger noise is an obvious contamination of data. Given the timing of the signal, however, it does not necessarily

interfere with seeing a cosmic muon signal. Cosmic runs are therefore suitable for correlating events and tracks between the two detector systems.

4.3 Time Stamps on TPC Data and Matching to Telescope Event Times

For the raw data, the first part of the time stamp is given as seconds since the Unix epoch, meaning January 1st, 1970 at 12:00 AM. The second part of the time stamp is the number of nanoseconds into the second. This precision of timing is not necessarily needed to correlate telescope event data but is used nonetheless. As with the muon GPS information, times are given in GMT (Greenwich Mean Time), which is six hours ahead of MST (Mountain Standard Time) at Los Alamos National Lab where the data is taken.

Only the cosmic runs provide data that can be correlated with the muon telescope. The pulsar do not trigger on any cosmic muon data. I verified this by looking at how many events were recorded in a given time interval, and I reported this issue to the CAPTAIN collaboration. Fortunately, several cosmic runs were done in March so my procedure for matching telescope and TPC time stamps could be tested.

Time stamps on TPC events are vital for matching the correct good event from the telescope data's fit track. For the first argon fill in October of 2014, the TPC event time stamps were absent from all data taken. This bug in the DAQ's code was fixed by Clark McGrew before the second fill in February of 2015.

Since TPC time stamps are written by the computer and are not GPS times like the telescope, it was assumed there may be a small discrepancy between the two detector systems' times. In comparing the event times between the two systems, no events were

found to match. Instead of simply looking at times, I looked at time differences between subsequent events. By matching time differences I eventually figured out that the clocks were out of sync by 16 seconds (15.9912 seconds average difference). If this amount is subtracted from the telescope time stamp, then event times consistently match within a couple of milliseconds.

As it turns out, the 16 second time offset only applies to ubdaq files for the February data set. I found that the March data set has a 13.6 second offset instead. There are not enough cosmic runs over a long enough period to characterize the change in time differences, so with each new data set the offset needs to be recalculated. This could be done automatically with a program, but I simply look at the time differences between subsequent events to calculate the offset by hand.

4.4 Finding Hit TPC Wires from Telescope Tracks

I have demonstrated that event times in ubdaq files can be matched with GPS information of good telescope events. The next step is to calculate which TPC wires for matched events should have been hit using the telescope's fit track. It is first vital to understand the orientation of the wires for each TPC plane so that equations describing the n^{th} wire can be derived. These equations are used to calculate the intersection point between each wire and the fit track. If the intersection point is within the TPC volume and below the plane for a particular wire, then a hit is declared. A list of hit wires for each event is written out at the end of my program so that collaborators analyzing the TPC data have a more targeted search. I also provided them code to read the output ROOT tree.

Consider the geometry and orientation of each wire plane in the coordinate system. Figure 4.5 shows the wire planes with respect to the coordinate axes. Now equations describing the n^{th} wire can easily be derived, and an event display of hit wires can be drawn.

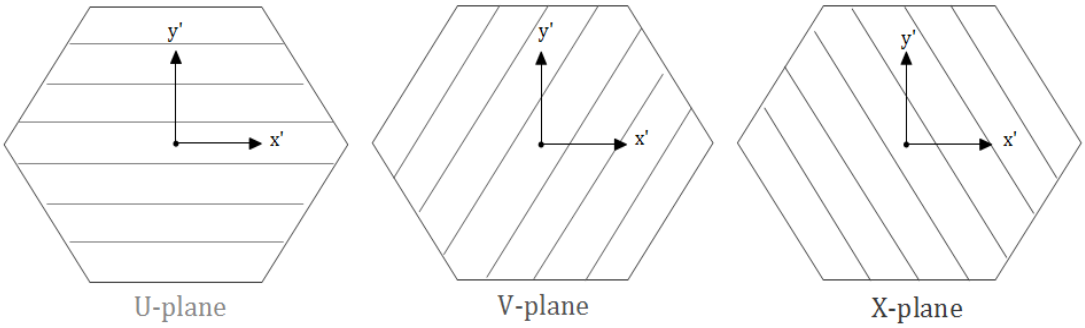

Figure 4.5 – TPC Planes, Wire Orientation in Coordinate System

To aid in the derivation, consider figure 4.6, where the middle and end wires of the V-plane have been drawn. The *y*-intercepts of the left-most and right-most wires are clearly seen to be at ±2*R*, and the slope is simply *2R/S*. Noticing that the *y*-intercept increases from *-2R* to *+2R* in consistent, small increments, allows the intercept as a function of *n* to be easily found (it is just a matter of keeping the wire numbering convention in mind).

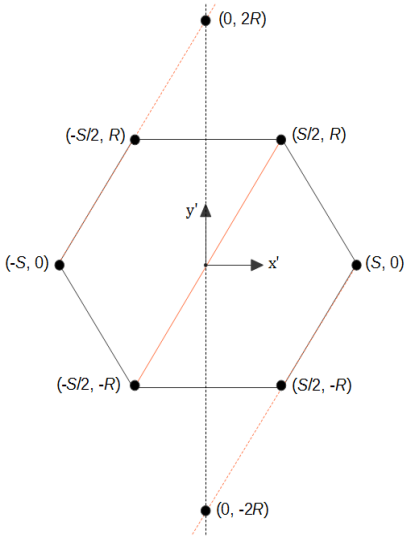

Figure 4.6 – Finding Y-Intercepts of V-Plane Wires

The following are linear equations describing the n^{th} wire for the U, V, and X planes. Note the domain and range per wire is implicitly within the hexagonal TPC frame shown in figure 4.6.

$$y_n' = R - \frac{(n-1)}{334} 2R \qquad \text{U-plane} \qquad (4.1)$$

$$y_n' = 2\frac{R}{s} x' - 2R + \frac{(n-336)}{334} 4R \qquad \text{V-plane} \qquad (4.2)$$

$$y_n' = -2\frac{R}{s} x' - 2R + \frac{(n-671)}{334} 4R \qquad \text{X-plane} \qquad (4.3)$$

Each plane has a range of n that is given in figure 4.2, meaning

$$1 \le n \le 335 \quad \text{for U-plane,}$$

$$336 \le n \le 670 \quad \text{for V-plane, and}$$

$$671 \le n \le 1005 \quad \text{for X-plane.}$$

As mentioned, these equations are defined so that the y-intercept is incremented by a small amount when increasing the wire number n. Plugging in values of n for the first and last wire in each plane is a simple way to check that the equations are accurate, as can be done with the V-plane by looking back at figure 4.6. The y-intercept for the top and bottom wires on the U-plane is also easily verified. Using eqn 4.1 gives $y_1' = R$ and $y_{335}' = -R$, which correctly describe the horizontal wires at the top and bottom of the hexagonal face in 4.6.

Now that equations describing the position of all wires have been determined, the intersection point of each wire with the muon telescope's fit track can be calculated. For the fit track equation, two points along the track are needed. I define (x_1', y_1') as the entry point of the fit track into the TPC and (x_2', y_2') as the exit point out of the TPC. In reality any two points along the fit track can be used, but this choice is made for convenience.

The equation for the telescope fit track is then given by the following.

$$y' = \frac{(y_2' - y_1')}{(x_2' - x_1')} x' + \frac{(x_1' y_2' - x_2' y_1')}{(x_1' - x_2')} \tag{4.4}$$

Equations 4.1 through 4.3 are set equal to eqn 4.4 so that the intersection point can be calculated, defined as (x_w, y_w). If this point is within the plane of the hexagonal TPC face, I check if z_w is beneath the TPC wire plane (for the appropriate plane) and above the bottom of the TPC. This tells me whether the intersection point (x_w, y_w, z_w) of each TPC wire with the telescope track is within the fiducial volume. If it is, then that wire is said to be hit.

The muon fit track is calculated in telescope coordinates, but the wires are described in TPC coordinates. Therefore, before proceeding to the main calculation, the general coordinate transformation is needed, where "general" means assuming an arbitrary rotation and translation. In figure 4.7 the coordinate axes for both detector systems is shown, and the distances t_y and t_z for the linear translation are labeled. It will be assumed that the yz and $y'z'$ planes are in the plane of the page, thus $t_x = 0$.

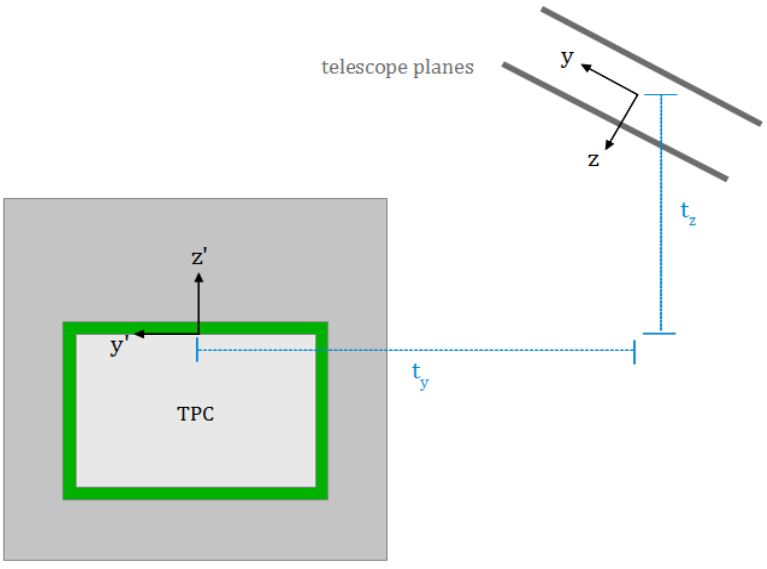

Figure 4.7 – Telescope to TPC Coordinate Transformation

Working out the general coordinate transformation is now simple using figure 4.7. First, the rotation matrices are defined. Rotation matrices are defined with the right-handed (counter clockwise) convention:

$$R_x = \begin{pmatrix} 1 & 0 & 0 \\ 0 & \cos(\theta_x) & -\sin(\theta_x) \\ 0 & \sin(\theta_x) & \cos(\theta_x) \end{pmatrix} \tag{4.5}$$

$$R_y = \begin{pmatrix} \cos(\theta_y) & 0 & \sin(\theta_y) \\ 0 & 1 & 0 \\ -\sin(\theta_y) & 0 & \cos(\theta_y) \end{pmatrix} \tag{4.6}$$

$$R_z = \begin{pmatrix} \cos(\theta_z) & -\sin(\theta_z) & 0 \\ \sin(\theta_z) & \cos(\theta_z) & 0 \\ 0 & 0 & 1 \end{pmatrix} \tag{4.7}$$

I define matrices X and X' to represent a point in the telescope and TPC coordinate systems, respectively. Also I define the linear translation matrix as T.

$$X' = \begin{pmatrix} x' \\ y' \\ z' \end{pmatrix} \quad , \quad X = \begin{pmatrix} x \\ y \\ z \end{pmatrix} \quad , \quad T = \begin{pmatrix} T_x \\ T_y \\ T_z \end{pmatrix} \tag{4.8}$$

With these definitions, a general coordinate transformation can be written as

$$X' = R_x R_y R_z X + T \tag{4.9}$$

Performing the matrix multiplication in the right side of eqn 4.9 is simplified by ignoring the rotation R_z. This leaves the problem general enough while giving simpler equations. Such a simplification is justified since $\theta_z = 0$ is a reasonable condition, as it is just a matter of proper telescope alignment. The task is now to evaluate eqn 4.10.

$$X' = R_x R_y X + T \tag{4.10}$$

The primed coordinates *X′* in terms of the unprimed coordinates X are found to be

$$x' = x\cos(\theta_y) + z\sin(\theta_y) + t_x \tag{4.11}$$

$$y' = x\sin(\theta_x)\sin(\theta_y) + y\cos(\theta_x) - z\sin(\theta_x)\cos(\theta_y) + t_y \tag{4.12}$$

$$z' = -x\cos(\theta_x)\sin(\theta_y) + y\sin(\theta_y) + z\cos(\theta_x)\cos(\theta_y) + t_z \tag{4.13}$$

As an example physical setup, consider the plane to be titled at θ_p = 45 degrees (recall figure 3.4), which means $\theta_x = \pi/4$ and $\theta_y = \pi$. Assume that $t_x = 0$ (as should always be the case if the telescope is lined up properly with respect to the TPC). For now, leave t_y and t_z generalized without plugging numbers in. To see a physical representation of these values, look back at figure 3.9. In that figure, the following values are used: $\theta_x = \pi/4$, $\theta_y = \pi$, t_x = 0 cm, t_y = -118.7 cm and t_z = 105.0 cm. This was the configuration in the actual telescope setup for the March data runs.

Plugging in $\theta_x = \pi/4$, $\theta_y = \pi$, and $t_x = 0$ into eqns 4.11 – 4.13 gives the following:

$$x' = -x \tag{4.14}$$

$$y' = \frac{1}{\sqrt{2}}(y + z) + t_y \tag{4.15}$$

$$z' = \frac{1}{\sqrt{2}}(y - z) + t_z \tag{4.16}$$

Next, I will write the primed coordinates solely in terms of the unprimed *z*-coordinate, the linear track fit constants (*A, B, C, D*), and the linear transformation constants (t_x, t_y, t_z). Doing so simplifies the subsequent calculations, as solving the equations is reduced to simply solving for the variable *z.* All primed coordinates can then be easily calculated.

After substituting expressions for $x(z)$ and $y(z)$ in eqns 4.14 – 4.16, I obtain the desired expressions for the primed coordinates.

$$x'(z) = -Az - B \tag{4.17}$$

$$y'(z) = \frac{1}{\sqrt{2}}(C+1)z + \frac{1}{\sqrt{2}}D + t_y \tag{4.18}$$

$$z'(z) = \frac{1}{\sqrt{2}}(C-1)z + \frac{1}{\sqrt{2}}D + t_z \tag{4.19}$$

Recall that by eqn 2.6 and 2.7 the fit constants A through D are determined by performing a linear fit on the muon telescope data. The equations describing the linear fit track are copied below for convenience.

$$x(z) = Az + B$$

$$y(z) = Cz + D$$

To continue the calculation, consider the intersection of the fit track with wires on the U-plane. These wires are geometrically described by eqn 4.1. Setting this equal to eqn 4.4 gives

$$\frac{(y_2' - y_1')}{(x_2' - x_1')}x' + \frac{(x_1' y_2' - x_2' y_1')}{(x_1' - x_2')} = r - \frac{(n-1)}{334}2\mathrm{r}$$

$$\frac{(y_2' - y_1')}{(x_2' - x_1')}(-Az - B) + \frac{(x_1' y_2' - x_2' y_1')}{(x_1' - x_2')} = r - \frac{(n-1)}{334}2\mathrm{r}$$

Next, solve for z.

$$(-Az - B) = \left(r - \frac{(n-1)}{334}2\mathrm{r} - \frac{(x_1' y_2' - x_2' y_1')}{(x_1' - x_2')} \right) \frac{(x_2' - x_1')}{(y_2' - y_1')}$$

$$z = \frac{-1}{A}\left(r - \frac{(n-1)}{334}2\mathrm{r} + \frac{(x_1' y_2' - x_2' y_1')}{(y_2' - y_1')} \right) \tag{4.20}$$

Finally, compute the value of z for the n^{th} wire and plug it into eqns 4.17 – 4.19. This gives the point of intersection, defined as (x_w, y_w, z_w). For the U-plane wires, the n^{th} wire is declared to be hit if the intersection point is within the TPC volume and if $z_w < z_{u\text{-}plane}$. The procedure is followed in a similar way for the V and X planes, though the algebra is a bit more lengthy since an x' term is introduced into the right hand side of eqn 4.2 and 4.3.

Hit wires are drawn using the existing event display code. A list of hit wires is kept, and a loop iterates through this list and draws the hit wires. The formula to calculate the start and end points of the wire depends on the range the wire number is in. Each plane is broken into two sections, so there are six different equations for the starting and ending point in terms of the wire number n and the geometric constants R and S. Displaying the hit wires is the best way to check that the calculated list of wires is correct and consistent with the TPC track.

An example event is drawn in figure 4.8. This is the same event as figure 3.11, but this time a top view of the TPC is shown with hit wires drawn. For this event, a a total of 243 wires between the three planes. The wire numbers for the hits are also shown in the figure. Recalling the legend in 3.11, the green line represents the telescope fit track, and the blue thicker line is the TPC track (i.e. the part of the fit track that goes through the TPC). In essence, all wires directly above the TPC track are declared hit, so looking at blue TPC track in the event display is the fastest and best way to verify the calculated hit wires are legitimate.

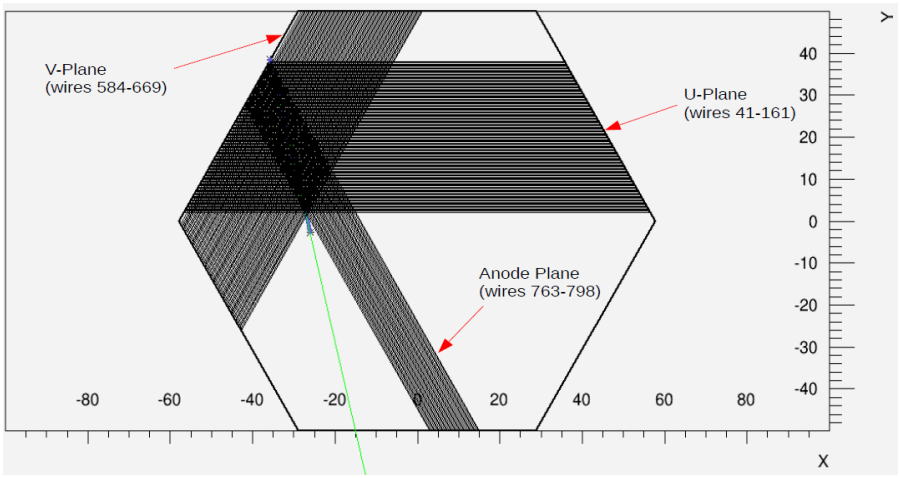

Figure 4.8 – A Track Drawn with Hit TPC Wires

A list of candidate wires is exported in a ROOT tree for the good events (where a good event is defined as one containing more than 10 hit wires). The output ROOT tree also contains the direction and location of the muon as it passes the anode plane. Additionally, GPS information for each good event is written in the same format as TPC time stamps (seconds since the Unix epoch and nanoseconds into that second). I correct for the offset in time stamps in the TPC analysis code since the offset can change from one data run to the other. Lastly, the vertical drift distance to each wire is calculated and written. This allows for an even narrower search of signals in TPC data, as wires with a small drift distance to the fit track are more likely to be hit (since the signal attenuates quickly in liquid argon without pristine purity).

4.5 Telescope Tracking Extrapolation into TPC

To understand the validity of the candiate wire list, it is important to quantify the fit track's uncertainty in position at each TPC plane. Only looking at the candidate wires could miss part or even all (in special cases) of the muon signal. For a very large uncertainty, such as 20 wires, I should look at data for the generated list and for the 20 wires on either side of the cluster of expected hit wires. The uncertainty will be different for each muon track and for each wire plane. A procedure for quantifying the tracking uncertainty for the U, V, and anode planes is discussed next.

Recall that the raw data from the muon telescope is used to determine the hit position with respect to the center of the wire plane according to eqn 2.1, and then the position is rounded to the nearest wire. Because of this the uncertainty of a wire hit is ±4 mm, or half a wire spacing. Each hit on all eight telescope wire planes has this uncertainty. The muon track reconstruction is first redone assuming that the wire hit on plane 1 is actually one wire over, which gives a slightly different muon trajectory. Next, the difference between the original muon location and the new fit track's location is computed at each TPC wire plane. This is done for all telescope wire hits in a given event, and then all of the differences are summed in quadrature. I expect the uncertainty at the U plane will on average be larger than that of the anode plane, as the muon travels farther to reach the U plane. The tracking uncertainty is therefore propagated over a longer distance.

To give an example, say the tracking uncertainty is 5 cm at the V plane along the direction parallel to the V plane wires. In this case, the candidate wire list for this plane would not really change. The obvious exception is if the modified track misses the TPC detection volume entirely. If instead the 5 cm uncertainty is instead perpendicular to the V

plane wires, then the track may have hit many wires away from the original track's intersection point Therefore, in under-standing the accuracy of the candidate wire list, it is the perpendicular distance to the TPC wires that is of interest.

To aid in visualizing the different TPC wire plane orientations with respect to a typical muon track, consider figure 4.9. Based on the track shown, the U plane would seem to have the largest uncertainty in the direction perpendicular to the wires. Based purely on a geometric argument, the uncertainty should be about twice as many wires for the U plane compared to the other two TPC planes. If the vertical angle of the track changes by a couple degrees, then the list of hit wires on the U planes changes the most dramatically, as does the drift distances to the U plane wires.

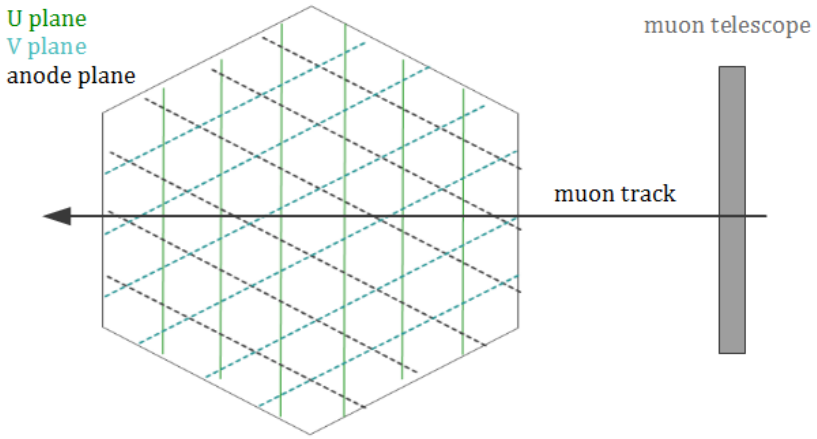

Figure 4.9 – Top View of Muon Track and TPC Wire Planes

Next, the uncertainties for the three TPC planes is quantified by analyzing telescope data from the March cosmic runs. Looking at 462 good events from March 14th 2014, I find that averaged uncertainty for the U, V, and anode planes are 3.2 cm, 2.9 cm, and 2.78 cm, respectively. Again the component perpendicular to the wires on each plane is used. For the anode plane, the largest calculated uncertainty in the 462 events is 4.9 cm, and the smallest

is 1.8 cm. Since TPC wires are spaced out by 3 mm, the averaged uncertainties are 10.7 wires, 9.6 wires, and 9.3 wires for the three planes. As expected, the V plane and anode plane have roughly the same uncertainty, and the U plane has the largest. As a check for consistency, I analyzed 1,156 good events from data taken March 3rd through 5th. This gave nearly identical results. As a general trend, the steeper the muon track's angle, the smaller the uncertainty. This is because the track intersects the TPC closer to the telescope, and hence the error is propagated over a smaller distance.

It is also useful to characterize the uncertainty for the electron drift distances. Looking at TPC wires with small drift distances (i.e. wire just above the muon trajectory) increases the likelihood of seeing a track. However, if there is a large uncertainty in the drift distance, then only looking at wires with small drift distance based on the original fit track may be insufficient. In the same way as before, the hit wire on each telescope plane is moved one wire over (so eight additional fits are performed). For each fit the difference between the new drift distance and the original is calculated, and all eight differences are summed in quadrature. Looking at the same 462 good events from March 14th, I found that a typical range in drift distance uncertainty is between 3 cm and 7 cm for a given event. Sometimes the range of uncertainty is even greater. The most promising wires are therefore not just those with a very small (say less than 2 cm) drift distance. It may also be useful to look at data from the TPC wires that are just beneath the original track or any of the modified trajectories.

4.6 Looking at Candidate TPC Wires

As detailed in section 4.4, a list of potentially hit TPC wires (candidate wires) is calculated based on the fit track generated by muon telescope data analysis. For cosmic runs, there is a one-to-one correspondence between TPC and telescope data, and I have demonstrated that time stamps can be used to match telescope events with TPC events. If a TPC event time-matches with a known good telescope event, then the list of candidate wires is retrieved. Technically, the wire number list is actually of channel numbers, which is done for convenience since the ubdaq files are ordered by channel.

The main goal in all of this effort outlined in chapter 4 is to narrow down the search for cosmic muon signals on TPC wires by calculating which one should have been hit by tracks through the muon telescope. The search can be narrowed down even more by calculating the vertical distance from the track to each wire i.e. the drift distance. Wires that have a small drift distance are much more likely to see a signal, especially if the purity is not optimal. If a signal is found in the TPC data, and the hit wires are those that should have been hit according to the telescope data analysis, then much more confidence can be placed in claiming that a muon track has been seen through the TPC. The last part is essential since it is the last step in commissioning the mini-CAPTAIN detector.

Next I consider the cosmic runs from March of 2015. After analyzing the telescope data and generating the output root file, I run my analysis program for the TPC data files. Out of 675 cosmic events recorded over three runs on March 5th, there are eight events that time-match with good telescope events. In these eight events there are typically around 100 candidate wires. Plots are generated (VDC counts vs. TDC counts) for every candidate wire and examined individually. Recall TDC means time to digital conversion, and so VDC means

voltage to digital conversion. For now there is no benefit in converting the voltage counts and time counts into actual units of volts and seconds, so the raw data itself is plotted.

Unfortunately, most of the plots generated from the eight matched events show no signs of a muon signal. All channels are eventually plotted and examined to be thorough. There are some signatures of signals, though nothing that can be called a muon track. It is important to look at the peak width, timing with respect to the trigger, and whether the same peak is seen at the same place from event to event (which indicates electronic noise if so).

Perhaps the most interesting event from the first three cosmic runs in March is event 200 in run 4045 (run number comes from the online mini-CAPTAIN elog maintained by LANL). A bipolar signal is seen on channels 257-260, with the magnitude decreasing with increasing channel. These channels are in the U plane, the first of the two induction planes that collect data, and they are among the expected channels to have a muon signal based on telescope data analysis.

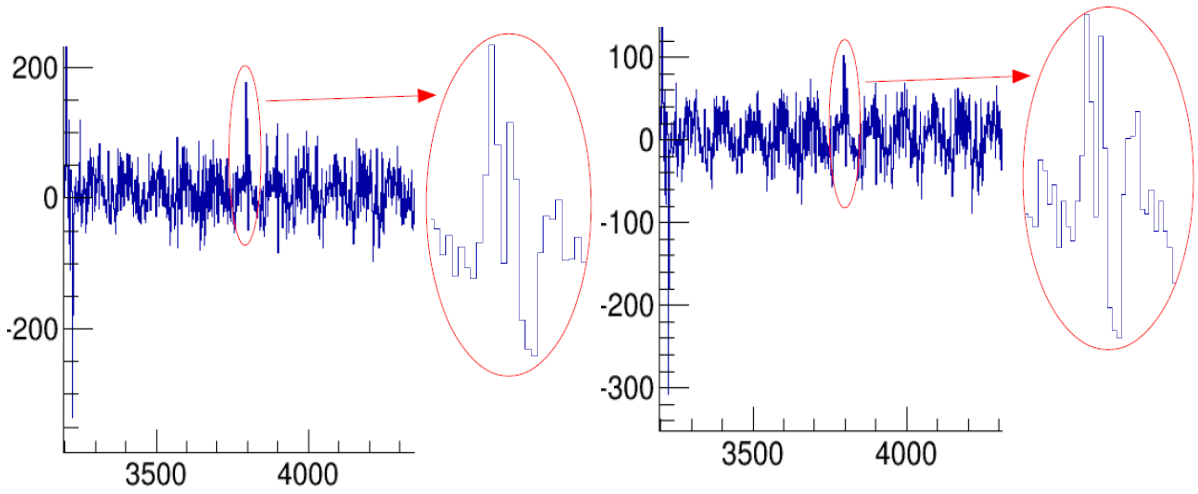

Figure 4.10 – Feature on Channels 257 (left) and 258 (right)

Recall that the trigger window is from 3196 to 6392 TDC counts, and so I only plot this time interval. As a muon continues its downward trajectory through the TPC, the drift distance of the ionized charge increases, hence the signal will become more attenuated. This feature can be seen in figure 4.10, where ch 257 has a peak magnitude of 175, which is larger than ch 258's peak value of 100. The peak continues diminishing across channels 259 and 260, as seen in figure 4.11, with values of 80 and 65, respectively. Channel 260's peak is barely larger than the neighboring noise pulses and hardly looks bipolar.

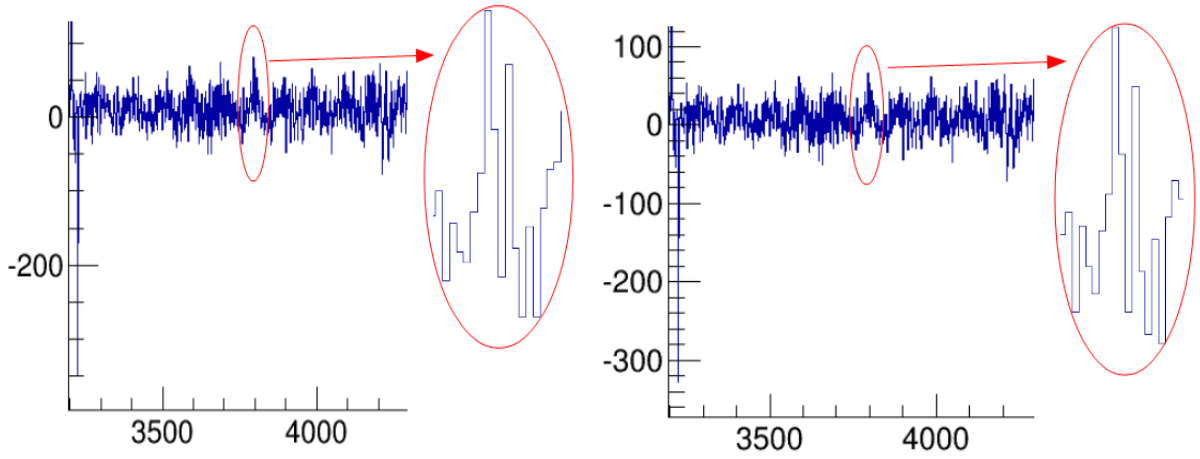

Figure 4.11 – Feature on Channels 259 (left) and 260 (right)

Is this a signal from a cosmic muon? It is difficult to say definitively, but it seems unlikely. There are two good reasons that cast doubt. First, a muon signal diminishes in order of physical wire number, not electronic channel number. A pulse of electronic noise, however, would more plausibly diminish by channel number order. The second reason is that some time shift of the signal is expected from wire to wire, since charge generated further down the muon track starts at a lower position and hence takes longer to drift up to the wires. It is not obvious by the plots in figure 4.10 and 4.11, but the highest point in each

plot is actually in the same two time bins. This is equivalent to a 1 μs interval. If a muon is moving downward at a 45 degree angle, then the difference in charge arrival time for neighboring wires could be as great as 1.88 μs (assuming a drift velocity of 1.66 mm/μs). On the other hand, an electronic signal moves much faster and would be expected to occur at the same time for all channels with the same noise pulse.

Looking at telescope data from March 5th to the 8th, I found 1,029 good events out of 79,900 total events. This means about 1.3% of events triggered on the muon telescope actually penetrate the TPC planes. Geometrically speaking, this is very reasonable, as many tracks go off to the left or right of the TPC or are not at the correct angle. More cosmic runs were performed in the middle of March, with run 4103 containing around 7,000 events. There are 115 time-matched events, which is by far the most coincident events in a single cosmic run. In this run the good event rate is roughly one event every three minutes. Amongst the 11,593 plots generated by my TPC data analysis program, there is nothing that particularly looks like a cosmic muon signal. Yujing Sun from the University of Hawaii at Monoa also looked at these runs and shared plots of possible signals with the collaboration. It was decided that a signal had not been seen., but more data is coming in the summer of 2015. To better our chances of quickly finding a signal, more sophisticated signal searching techniques are being developed.

4.7 Techniques for Finding Hit Wires in TPC Data

Besides simply looking at each plot for candidate wires, better methods can be used to find cosmic muon signals in the TPC data. Before discussing specific techniques, it would be useful to understand what a muon signal should look like. For the induction planes, a symmetric bipolar is generated as charge drifts by the wires. The signal width is three to four μs. For the collection plane, a mono-polar signal with the same width is generated when charge arrives. Pulse height depends on the muon's energy. Besides the shape, it is also important to understand the timing with respect to the trigger window. The peaks highlighted in figure 4.10 arrived too late to be a muon signal.

With almost 1,000 wires and 1000s of events to look at, more sophisticated techniques are required to sift through all the data and hone in on the most promising events and channels. By developing algorithms to subtract periodic noise (both high and low frequency), peaks from a muon signal become more prominent. This does not, however, help with problems of random noise or static discharge on wires. Algorithms can also be developed for finding peaks. Yujing Sun from the University of Hawaii at Manoa has employed such strategies. With better signal finding techniques, along with lower noise and better purity, cosmic muon tracks should be found in the new data coming out in the summer of 2015.

CHAPTER 5: SUMMARY AND CONCLUSIONS

I have demonstrated that cosmic muon events can be reconstructed with mini-CAPTAIN's muon telescope and that they can be correlated with TPC events. A larger fraction of data could be correlated after the telescope was repositioned, a decision that was in part supported and motivated by my study of finding the optimal telescope location. For the telescope tracks that are found to intersect the TPC, a list of TPC wires that should see a muon signal is generated. The list of candidate wires, along with the vertical distance from the track to each wire (i.e. the electron drift distance), is written to a ROOT file. Also included in the file is the event time and the track's direction at the anode plane. After analyzing the telescope data, a separate program is used to step through the TPC data files. When a TPC event is time-matched with a known good telescope event, the list of candidate wire is retrieved from the ROOT file. The raw data from these wires is then plotted and analyzed for signs of a cosmic muon signal.

While a full muon track through the TPC has not been found, the collaboration is hopeful that new data coming in the summer of 2015 will reveal tracks, hence completing the commissioning phase of mini-CAPTAIN. From there, the collaboration will shift focus to CAPTAIN. Many tasks must be completed for CAPTAIN, including the construction of its TPC, which will be carried out by the UCI group. As mentioned in section 1.1, the future experiments DUNE and LBNF are supported by studies that will be performed by CAPTAIN. It is therefore of the up-most importance to commission mini-CAPTAIN as quickly as possible.

BIBLIOGRAPHY

[1] A. Bettini, et al. "The ICARUS Liquid Argon TPC: A complete Imaging Device for Particle Physics." *Nuclear Instruments and Methods in Physics Research*, 1992.

[2] DUNE. [Online]. http://www.dunescience.org

[3] MINVERvA and CAPTAIN Collaborations. *CAPTAIN-MINERvA: Neutrino-Argon Scattering in a Medium-Energy Neutrino Beam.* 21 December 2014.

[4] The CAPTAIN Detector and Physics Program. [Online] http://arxiv.org/abs/1309.1740

[5] J. Beringer, et al. (Particle Data Group), Phys. Rev. D86, 010001 (2012).

[6] Orwig, Jessica. "Time Projection Chambers: a Milestone in Particle Detector Technology." *Symmetry Magazine*. October 2012.

[7] LArTPC in Brief. [Online]. http://www-lartpc.fnal.gov/summary.htm

[8] Lee, Dave et al. "A Memo on the First Data from Mini-CAPTAIN." 22 October 204.

[9] Scintillation and Light Sensitive Detectors. [Online.] http://neutron.physics.ucsb.edu/docs

[10] L.G. Atencio et al. "Delay-Line Readout Drift Chambers," *Nuclear Instruments and Methods*, vol. 187, 1981.